The Pennsylvania State University

The Graduate School

BENEFITS OF PARALLEL HYBRID ELECTRIC PROPULSION FOR AIRCRAFT AND ROTORCRAFT

A Thesis in

Aerospace Engineering

by

Dalton Decerio

Submitted in Partial Fulfillment
of the Requirements
for the Degree of

Master of Science

May 2022

The thesis of Dalton Decerio was reviewed and approved by the following:

David K. Hall
Assistant Professor of Aerospace Engineering
Thesis Advisor

Edward Smith
Professor of Aerospace Engineering

Karen Ann Thole
Distinguished Professor of Mechanical Engineering

Amy Pritchett
Professor of Aerospace Engineering
Head of the Department of Aerospace Engineering

ABSTRACT

As interest in the reduction of the environmental impact of commercial aviation grows alongside the continued pursuit of improved efficiency, electrification of aircraft propulsion systems may have potential to reduce the energy consumption and emissions of aircraft. Incorporating electrical components adds a dimension to the propulsion system design space and introduces new tradeoffs between weight and efficiency. In this thesis, we apply numerical optimization to conceptual design of regional transport category turboprop airplanes and light rotorcraft using geometric programming. A design optimization framework was developed for modeling hybrid propulsion systems in the context of vehicle conceptual design and used to evaluate the benefit over conventional systems, optimal operation strategy, and design changes with changes in electrical technology improvements. The objectives of this research are to quantify the energy savings benefits of parallel hybrid electric propulsion, identify the mechanisms of the benefits, and characterize the scaling effects of design parameters such as range and electrical technology parameters such as battery specific energy. The results show incorporation of current state-of-the-art electrical components may provide energy savings up to 7.7% over conventional turboprop engines, while projected improvements in technology may allow savings of up to 14.1%, albeit at a reduced range relative to conventional gas turbine powered aircraft. The rotorcraft considered differ from transport aircraft in that they are capable of vertical takeoff and landing which require higher power relative to cruise; rotorcraft with short-duration hover missions may save up to 12.7% energy using parallel hybrid electric propulsion systems with state-of-the-art

technology and up to 25.3% with projected technology improvements. By supplementing the gas turbine engine with electrical power in high-power conditions, the overall efficiency of the propulsion system can be improved throughout the mission. Improvements in battery specific energy and power electronics specific power have the largest impact on improvements in energy savings, and thus they are identified as enablers for efficient hybrid electric aircraft propulsion.

TABLE OF CONTENTS

LIST OF FIGURES

LIST OF TABLES

LIST OF SYMBOLS

Symbol	Description
A	Area
$\mathrm{AR}_{\mathrm{wing}}$	Wing aspect ratio
b_{wing}	Wingspan
BSE	Battery specific energy
C_{D_0}	Aircraft zero-lift drag coefficient, rotor blade drag coefficient
C_{D_i}	Induced drag coefficient
C_{f_e}	Equivalent skin friction coefficient
$C_{L_{\mathrm{TO}}}$	Takeoff lift coefficient
C_D	Drag coefficient
C_L	Lift coefficient
C_{max}	Battery maximum discharge rate
C_{P_o}	Profile drag coefficient
D_i	Corrected flow per unit area at station i (see Figure 2-2)
d_{prop}	Propeller diameter
$\mathrm{DOD}_{\mathrm{max}}$	Battery depth of discharge
e	Oswald efficiency factor
E_{batt}	Effective battery energy capacity
$\mathcal{E}_{\mathrm{batt}}$	Battery internal voltage
f_{empty}	Empty weight fraction not including engines or battery
F_{net}	Total force produced by propulsion system
F_{prop}	Propeller thrust
FOM	Propeller figure of merit
g	Acceleration due to gravity at sea level
h_{cruise}	Cruise altitude
h_{fuel}	Specific energy of jet fuel
h	Altitude
I	Current
k_{mot}	Motor mass scaling factor
k	Drag parametric scaling factor
ℓ_{cable}	Cable length
$\ell_{\mathrm{TO,max}}$	Maximum takeoff distance
M	Mach number
$\mathcal{M}_D$	Drag margin factor
m	Mass
N_{eng}	Number of engines
N_{prop}	Number of propellers connected to gearbox
$\mathrm{OPR}_{\mathrm{max}}$	Max compressor pressure ratio
P_i	Main rotor induced power

P_o	Main rotor profile power
P_p	Main rotor parasite power
P^*	Corrected power
P	Power
p_t	Stagnation pressure
p	Static pressure
Q	Heat rejected
q	Dynamic pressure
R_{gas}	Specific gas constant of air
R	Resistance, range
r_{hub}	Propeller hub radius
R_{mr}	Main rotor radius
r_{tip}	Propeller tip radius
S_{ref}	Wing reference area
S_{wet}	Wing wetted area
T_{max}	Motor maximum torque
T_{mot}	Motor torque
T_{mr}	Main rotor thrust
T_t	Stagnation temperature
T	Static temperature
u	Flow velocity
V	Voltage
v_{cruise}	Cruise true airspeed
v_i	Rotorcraft induced velocity
v_{tip}	Rotor tip speed
η	Efficiency
π	Pressure ratio
Ω	Angular speed
γ	Ratio of specific heats
ρ	Air density
σ	Rotor solidity, air density ratio
δ	Ratio of stagnation pressure to sea level static
θ	Ratio of stagnation temperature to sea level static
$\left(\frac{m}{A}\right)_{\text{gg}}$	Gas turbine engine mass scaling factor
$\left(\frac{m}{\ell}\right)_{\text{cable}}$	Cable mass per unit length
$\left(\frac{m}{d^3}\right)_{\text{prop}}$	Propeller mass scaling factor
$\left(\frac{R}{\ell}\right)_{\text{cable}}$	Cable resistance per unit length
$\left(\frac{P}{m}\right)_{\text{PE}}$	Power electronics specific power

PREFACE

Much of the research included in my thesis is based on “Benefits of Parallel Hybrid Electric Propulsion for Transport Aircraft”, a paper authored by myself and my research advisor, Dr. David Hall. As of the writing of this thesis, the paper is under review for publication in the 2022 IEEE Transactions on Transportation Electrification, Special Issue on Electrified Aircraft Technologies. I am the first author on the paper, and my contributions include the following: development of electrical component, gas turbine, mission, hybrid propulsion system, and aircraft level models, generation and analysis of numerical results, and drafting and editing the paper. This thesis includes content from the paper, and it expands on the work in the paper with a more comprehensive literature review, model description, and hybrid electric rotorcraft analysis.

ACKNOWLEDGEMENTS

I would like to thank my advisor, Dave Hall, for his continued guidance and support throughout my graduate studies and research. From my first introduction to GPKit and debugging the thousands of lines of code in the model, to encouraging me to develop and exercise my technical presentation and writings skills, you have been an invaluable resource.

Thank you to my colleagues in the Aircraft Propulsion Research Group, especially Aaron VanLandingham and Matt Ibasitas for their help workshopping presentations and developing rotorcraft modelling capabilities.

Lastly, thank you to my friends and family for supporting me throughout my time here at Penn State, and for the many memories I will look back on fondly in the years to come.

This material is based upon work supported by the U.S. Department of Defense under Award No. W911W6-21-2-0002. Any opinions, findings, and conclusions or recommendations expressed in this publication are those of the author(s) and do not necessarily reflect the views of the U.S. Department of Defense.

Chapter 1

Introduction

Hybrid-electric propulsion has been proposed as a way to improve aircraft efficiency and reduce the environmental impact of aviation. In this thesis, we assess the benefits of parallel hybrid electric propulsion, an architecture where batteries and electric machines provide mechanical shaft power that is combined with turbine shaft power. The analysis is carried out for regional transport turboprop aircraft and light rotorcraft using conceptual design models for vehicle and propulsion system sizing and performance, implemented in an optimization framework to minimize energy consumption. The models are used to quantify the energy savings provided by parallel hybrid propulsion, understand the mechanisms of the energy savings, and examine the scaling of the energy savings with mission and technology parameters.

1.1 Background

1.1.1 Environmental Impact of Civil Aviation

Electrified aircraft propulsion has been proposed in recent years as a way to improve propulsion system efficiency and reduce aviation greenhouse gas emissions. In 2016, the aviation industry was responsible for about 2% of CO_2 emissions. If the aviation sector continues to grow at 4% per year, however, aviation could account for 16% of the world's fossil fuel emissions by 2050 [1]. In 2016, the National Academy of Science, Engineering, and Medicine conducted a consensus study [2] with the goal of

assessing the state of emissions in aviation and developing a research agenda for the reduction of the carbon emissions of commercial aviation. Of the emissions associated with civil aviation, single aisle jets account for about 36% while twin aisle jets account for about 57%; the vast majority of aviation emissions are a result of commercial transport aircraft. There are three possible ways to reduce the carbon footprint of commercial aviation: reduce the energy required to fly aircraft by reducing weight or drag, improve the efficiency of aircraft propulsion systems, or reduce the emissions associated with each unit of energy input to the aircraft, whether it be fossil fuel or electricity [2].

While the fundamental mechanisms of carbon footprint reduction are clear, the study identified systemic and technical challenges in implementing emissions-reducing technology. Commercial aviation is a competitive industry and technological advancement is often driven by reductions in cost. Sometimes, this interest is aligned with the reduction of emissions; for example, fuel costs are a large percentage of airline operating costs, and reducing fuel burn reduces both cost and emissions. This is not always the case, however, as aircraft costs, maintenance, and other operations expenses must also be taken into account and may not align with what is best for the environment. The strict regulation of aviation requires that new technologies are thoroughly tested and evaluated to ensure the safety and performance of the aircraft and other critical systems are not compromised, making integration of new technologies more difficult and expensive. With these challenges in consideration, the 2016 consensus study identified advances in aircraft-propulsion integration, improvements in gas turbine engines, development of turboelectric propulsion systems, and advances in alternative jet fuels as

the four highest priority areas of research for the reduction of commercial aviation carbon emissions.

1.1.2 Electrified Aircraft Propulsion

Electrified aircraft propulsion leverages the efficiency of electrical components to improve propulsion system efficiency and allows for emission reductions by using energy from an increasingly renewable grid. With current battery technology, however, replacing a large aircraft's fuel entirely with batteries results in an increase in vehicle weight and the required energy [2], [3]. The goal of hybrid electric aircraft is to improve propulsion system efficiency while mitigating the energy penalty resulting from the added weight of batteries and other electrical components.

Unlike electric ground vehicles, transport category airplanes[1] do not benefit from replacing hydrocarbon-based fuel with batteries, due to the low relative specific energy of the latter and the sensitivity of aircraft performance to weight. Epstein and O'Flarity [4] examined all-electric, battery-powered aircraft with capabilities comparable to today's commercial fleet and found that they are not technologically feasible in the foreseeable future. Electrified aircraft propulsion runs into technical issues with the weight, efficiency, and thermal management of electrical components due to the large power and energy levels required by transport aircraft. Significant economic and policy changes

[1] Defined as multi-engine airplanes with more than 19 seats or a maximum takeoff weight greater than 19,000 lb.

would also be required to support a large-scale transition to electrified transport aircraft. As a result of these technical and systemic challenges, the authors concluded that fully-electric propulsion is unlikely to provide substantial emissions reductions to large commercial aircraft by 2050.

Incorporating electrical energy storage and power distribution into the drivetrain is not all-or-nothing, however; electrification adds new dimensions to the propulsion system design space and has led to a variety of proposed electrified propulsion concepts [1], [6]. Hall *et al.* [5] summarized vehicle performance for aircraft with electrified propulsion systems across a wide range of missions and propulsion system architectures, including turboelectric, fully-electric battery powered, and hybrid aircraft. Several of these propulsion system architectures use electrical power to enable aero-propulsive integration strategies such as boundary layer ingestion and distributed propulsion. The results showed that aero-propulsive integration could provide improved performance despite the weight penalty of the added electrical systems. Langford and Hall [6] discussed the benefit of several electrified system architectures, including all-electric, turboelectric, and hybrid configurations, and performed a case study on the retrofit design of a conventional aircraft with hybrid and fully electric propulsion systems. A cruise performance analysis showed that electrification can provide energy savings for short missions but reduce the range of the aircraft. They also mentioned the utility of electrification for propulsion-airframe integration such as boundary layer ingestion and blown lift. They concluded that battery-powered propulsion is only suitable for small, short-range aircraft and that aero-propulsive integration could lead to benefits for larger

commercial transport aircraft and identified hybrid systems for improved gas turbine engine efficiency as an area for future research.

Hybrid-electric concepts may offer the best opportunity for fuel, energy, and emissions reduction by leveraging the combined benefits of gas turbine and electric power systems. There are several implementations of electrified aircraft propulsion systems, including hydrogen powered, turboelectric, series hybrid, and parallel hybrid, summarized in Figure 1-1.

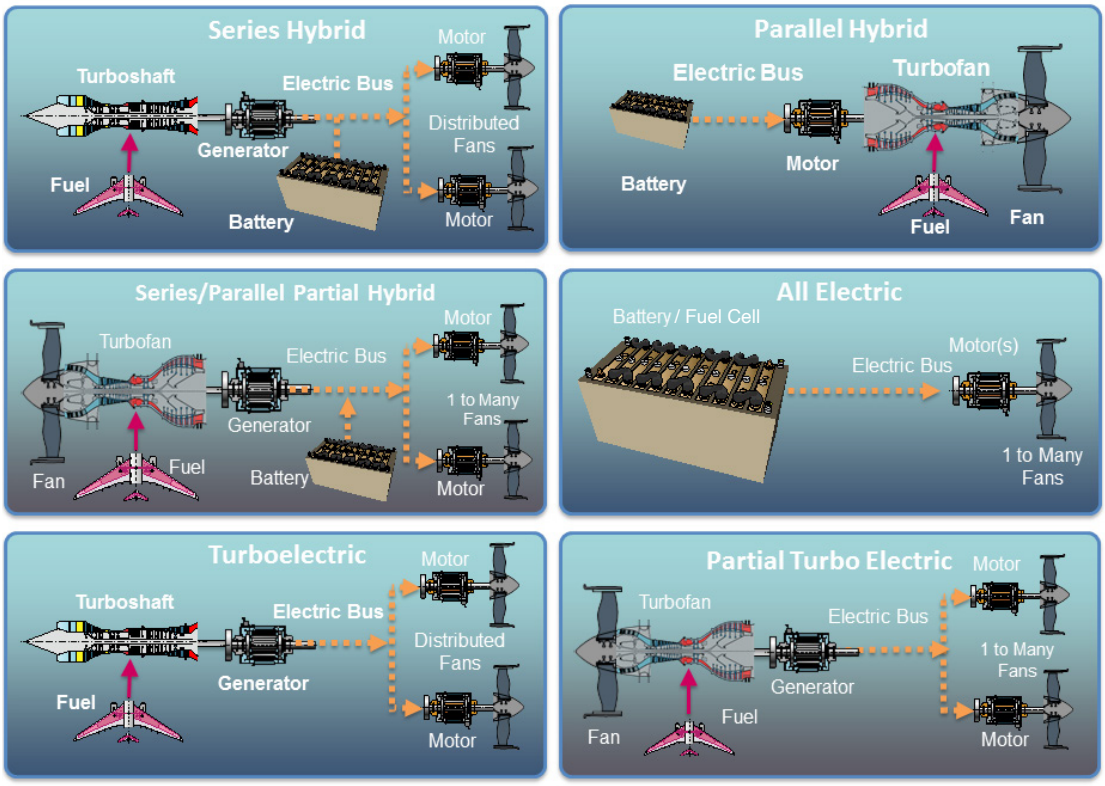

Figure **1-1**: Electrified propulsion architectures [2]

As described above, fully battery powered aircraft are unlikely to be feasible for transport aircraft, but fuel cell systems may enable all-electric architectures using fuels with higher specific energy. Hydrogen fuel cell powered aircraft produce electricity from

liquid hydrogen and power many motors to turn propellers or fans. Hydrogen fuel cells systems require large thermal management systems and are not volumetrically energy dense, but advanced fuel cell technology may prove valuable in reducing the carbon emissions of commercial aircraft. In a study on hydrogen-powered aviation, McKinsey & Company [7] predicted that possible advances in hydrogen fuel cell technology in the next 10 years may provide the potential for up to 90% reduction in aviation emissions at the cost of a price increase of up to 30% per customer.

Turboelectric aircraft use gas turbine engines to turn electric generators to provide power for electric propulsors. Although converting the mechanical energy to electrical energy and back leads to losses in efficiency, it enables the distribution of power to many propulsors, which may lead to improvements in propulsive efficiency through propulsion-airframe integration. De Vries, Hoogreef, and Vos [8] performed a conceptual design study to determine the electrical technology and aero-propulsive efficiency improvement, provided by propulsion-airframe integration. The authors found that electrical powertrain technology from approximately 2015 enabled an 11% increase in aeropropulsive efficiency, leading to a 5% reduction in energy consumption.

Series hybrid propulsion systems are similar to turboelectric but supplement the electrical power from turbine-powered generators with batteries. Parallel hybrid propulsion systems also use batteries to supplement gas turbines, but combine the mechanical power of the turbine with the power of an electric motor using a gearbox rather than using the turbine to power a generator. This removes the associated generator and motor efficiency losses and the ability to distribute power to many propulsors. Parallel hybrid electric propulsion is an attractive solution for retrofitting existing

conventional aircraft, and analyzing this implementation of electrification allows the benefit of hybridization to be isolated from the improvements in efficiency provided by distributed propulsion and boundary layer ingestion.

1.1.3 Parallel Hybrid Electric Propulsion

Parallel hybrid-electric propulsion, where gas turbine engine power is supplemented by a battery-powered electric machine, represents an incremental change in propulsion system architecture that minimizes additional weight and losses associated with additional electrical components. It also retains high energy density fuel as the primary energy source, using batteries for only a fraction of the overall mission energy. An overview of the parallel hybrid electric propulsion system studied in this thesis is included in block diagram form in Figure 1-2.

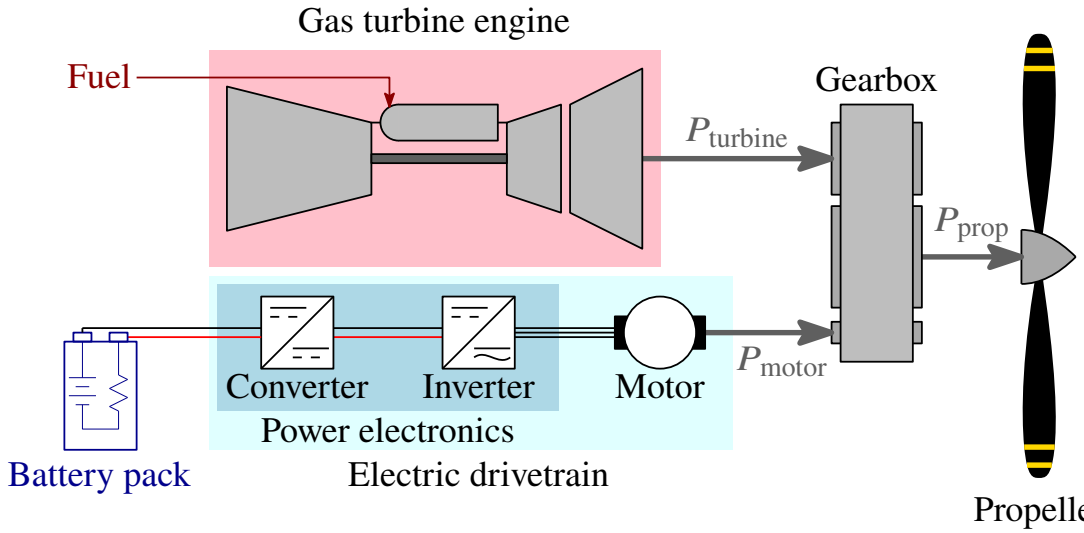

Figure **1-2**: Parallel hybrid electric turboprop propulsion system configuration model schematic.

Trade studies on the effect of cruise performance for fixed-wing aircraft have shown that parallel hybrid propulsion can improve overall energy efficiency at the cost of reduced range or payload capability, as shown in the previously mentioned studies [1] and [6]. Further, Kruger *et al.* [9] presented a design space exploration for aircraft utilizing electrified propulsion ranging from thin-haul to twin-aisle aircraft. The analysis presented used a generalized range equation for cruise-only analysis, and the authors found that increasing the size of the battery could provide energy savings at the cost of maximum range capability. The authors concluded that all-electric aircraft are beneficial for the short-range missions they are capable of, while hybrid-electric aircraft are capable of saving some energy for mid-range missions, and for longer missions, turboelectric configurations are beneficial for enabling distributed propulsion and propulsion-airframe integration.

More detailed studies and off-design analyses have shown that parallel hybrid systems can offer a benefit in performance by supplementing gas turbine power during short-duration operation at high thrust and providing a degree of freedom via electric control of the speed of the engine to optimize turbine engine component performance over the course of the mission. Simon, Connolly, and Cully [10] explored the challenges and opportunities associated with the control systems needed to integrate electrical components with gas turbine engines. The authors state that introduction of electric machines to the gas turbine can fundamentally change the design of the gas turbine in two main ways. Turbine Electrified Energy Management uses electric machines to add or extract power from the gas turbine during transient periods such that the turbomachinery components operate in steady-state at their optimal conditions. More Electric Engines

replace pneumatic and mechanically driven components with electrically actuated components to reduce the engine weight and improve overall engine efficiency. Richter, Connolly, and Simon [11] implemented an optimal control model to evaluate the benefit of Turbine Electrified Energy Management where the electrical energy and fuel burn are minimized subject to the gas turbine dynamics over operating conditions from past flight data. The authors found that the total mission energy could not be reduced due to losses in the electrical components, but suggest future research into optimal control strategies may improve the fuel burn reduction.

Without significantly altering the design of gas turbine engines, parallel hybrid electric propulsion systems can be used to provide energy savings for aircraft sized by short-duration power requirements. Finger, Braun, and Bil [12] assessed the benefit of parallel hybrid electric propulsion for aircraft including regional transports, general aviation aircraft, VTOL air taxis, and unmanned aircraft. The authors used an iterative design optimization process to size each aircraft and assessed the mission energy consumption, finding that parallel hybrid-electric propulsion is best suited for missions with sizing dominated by vertical takeoff or climb power requirements. The authors reported total energy savings of up to 65% and 38% for VTOL air taxis and UAVs respectively with optimistic technology assumptions, and no potential for energy savings for general aviation and regional transport aircraft.

Several other transport aircraft design studies *have* shown potential fuel or energy consumption reductions for parallel hybrid electric propulsion for transport category aircraft ranging from 2% to 60%, depending strongly on the size and range of the aircraft and assumptions about electrical component performance, particularly battery specific

energy. Bradley and Droney [13] designed five aircraft concepts and evaluated their performance, emissions, and technology risks. Among the concepts discussed is the SUGAR Volt, a parallel hybrid electric single-aisle jet with projected technology from the "N+3" timeframe, or about 2030. The authors also established both 2008 and N+3 baseline jets for comparison. Their analysis showed 63% and 30% reductions in fuel burn relative to the 2008 and N+3 baselines respectively for a 900 nautical mile mission, corresponding to approximately 56% and 15% reductions in total mission energy. Bradley and Droney [14] continued this research; they went on to explore multiple designs within the hybrid electric design space trading between total energy consumption and fuel burn reductions. They found similar results to [13], with the best design achieving a 60% reduction in fuel burn and a 54% reduction in total energy consumption. The authors also concluded that parallel hybrid electric propulsion allows a reduction in total lifecycle emissions depending on the source of the electricity used, a reduction in aircraft noise, and a reduction in the energy cost. They noted, however, that the energy cost savings are offset by the increase in cost due to the increased weight and complexity of the aircraft.

Lents and Hardin [15] designed a parallel hybrid single-aisle jet and evaluated two different concepts of operation. The hybrid aircraft's gas turbine engine was sized for cruise conditions, unlike the conventional baseline whose engine is sized for takeoff and top-of-climb, thus the hybrid aircraft must use electric power to supplement the gas turbine during high power conditions. In the first concept of operations, the aircraft had a battery onboard with enough energy stored just for takeoff and climb, and the aircraft takes off below its maximum takeoff weight (MTOW). With this concept, Lents and

Hardin reported a 3.4% reduction in fuel burn corresponding to a 0.6% increase in total energy consumption. In the second concept of operation, the aircraft had a large battery such that it can supply some of the energy during cruise and the aircraft takes off at its maximum takeoff weight. This concept of operation underperformed the other in both fuel consumption and total energy. Spierling and Lents [16] performed a similar analysis for a regional turboprop retrofit with a parallel hybrid propulsion system. Once again, the gas turbine was sized for the cruise power condition, with the electric drivetrain used to supplement the gas turbine engine during takeoff and climb, leading to a projected improvement in gas turbine engine efficiency of about 10% during cruise. The authors reported a fuel burn reduction of 30% and an energy consumption reduction of 25%.

The application of parallel hybrid electric propulsion to rotorcraft has been less widely studied. Rotorcraft have a wider range of applications than aircraft, with missions ranging from search-and-rescue to cruise-dominated transport. Similar to fixed wing aircraft, analyses have shown using parallel hybrid systems for missions with short periods of high rotor power requirements may allow an improvement in efficiency and a reduction in fuel burn. Rotorcraft may require as much as double the power during hover as they do during cruise at the optimal speed; rotorcraft performing missions with short periods of hover and long duration cruise may benefit from supplementation of the gas turbine engine with electrical power during hover, while rotorcraft performing missions consisting mainly of hover may not see as large of a benefit due to the weight of the battery needed to supply power during extended high-thrust periods. Danis *et al.* [17] performed a conceptual design study of a parallel hybrid electric rotorcraft based on the XV-15 and found possible fuel consumption savings of 10%. Saias *et al.* [18] performed

a similar study on the same aircraft, and found fuel consumption savings of 12%. Saias *et al.* also showed that parallel hybrid electric propulsion can increase the maximum range of rotorcraft by up to 50% by improving cruise efficiency, depending on the assumed battery specific energy.

1.1.4 Design Optimization

Design optimization is a frequently used method in engineering that employs mathematical models of systems for solving design problems. In an optimization problem, design variables that minimize a specific objective function are solved numerically. Common choices of objective function for the conceptual design of conventional aircraft include maximum takeoff weight and mission fuel burn; both of these parameters are relevant to the physical models of the system and are related to the cost of the aircraft, which the aircraft designer likely wants to minimize. Choosing the objective function is an important step in setting up an optimization problem, and there are often multiple competing objectives of a design problem. For the design optimizations in this thesis, the objective function used was *total mission energy*, including contributions from fuel and battery; more information on the chosen objective function can be found in Section 2.2.

Geometric programming (GP) is an optimization frameworks that has been used for aircraft and propulsion system conceptual design for both conventional and novel aircraft concepts. The mathematical form, advantages, and disadvantages of geometric programming are discussed in Section 2.1. Kirschen *et al.* [19] demonstrated the

effectiveness of signomial programming, a less restrictive form of optimization problem that can be solved using geometric programming techniques, for system-level design optimization modeling of commercial aircraft. Mathematical models that fit the required form for signomial programming were proposed for the sizing of the aircraft's wing, vertical and horizontal tail, fuselage, and landing gear. These models were coupled, and the mission fuel consumption, determined using an adaption of the Breguet range equation, was minimized. Kirschen *et al.* thoroughly detailed the process of creating signomial models and their advantages and disadvantages. York *et al.* [20] ran a benchmark to compare signomial programming to another multidisciplinary design optimization tool, Transport Aircraft System Optimization (TASOPT), for three sizes of commercial aircraft design optimization problems. The authors found that signomial programming was 16 to 39 times faster than TASOPT and demonstrated the reliability of signomial programming.

Geometric and signomial programming have also been used for the design of electrified aircraft concepts, including previously mentioned studies [4] and [8]. In another study, Burton *et al.* [21] applied geometric programming to the design of solar-electric aircraft by combining models for aerodynamic performance, structural integrity, component performance, and manufacturability. The optimization model was used to conduct trade studies on design parameters, and the results were used to both inform design decisions and validate the models used. The authors found that the speed and robustness of geometric programming was useful for performing extensive trade studies that may not have been feasible with traditional aircraft design optimization procedures. Courtin *et al.* [22] used geometric programming to minimize the weight of an all-electric

urban air mobility vehicle subject to short takeoff distance constraints. The aircraft takes advantage of distributed propulsion and blown lift to shorten the required takeoff distance, and optimization results indicated takeoff distances of 100 to 300 feet are feasible depending on the technology assumptions used; battery specific energy in particular is noted as a key enabling parameter.

Dowdle, Hall, and Lang [23] built turboelectric aircraft component models in the signomial programming framework and assessed them both individually and in the context of the entire propulsion system. Individually, the authors noted that components such as electrical cables and motors have a trade-off between reducing weight and improving efficiency – the more efficient a design is, the heavier it must be. In the propulsion system level context, optimal designs were analyzed for two objective functions: fuel consumption and propulsion system mass. The resulting designs were different, and the authors concluded that the optimal propulsion system design depends on the propulsion system architecture, the operating point under consideration, and the objective function, which suggests that novel propulsion systems must be assessed in the context of the entire aircraft and a representative mission.

1.2 Thesis Scope and Contributions

In this thesis, we *quantify the energy consumption reduction* enabled by parallel hybrid electric aircraft propulsion, *identify the mechanisms* of the benefit, and *assess the scaling* of the benefit with changes in mission and electric component performance. This is achieved using vehicle conceptual design framework where the aircraft, propulsion

system, and mission are optimized for minimum total energy consumption. The results show a modest reduction in mission energy consumption with supplemental electrical power during climb, which enables a smaller gas turbine engine with higher efficiency during cruise and reduced fuel consumption during all phases of flight, with greater reductions possible with decreased design range, increased battery specific energy, and increased electrical component specific power and efficiency. We limit the analysis to regional turboprop aircraft and light rotorcraft because the results show the benefits diminish with increasing range and propulsive power, even with projected improvements in electric component energy density, power density, and efficiency.

The contributions of this thesis are:

1. Development of a design optimization framework for parallel hybrid electric propulsion of aircraft and rotorcraft,
2. Assessment of the energy savings enabled by parallel hybrid electric propulsion for regional turboprop transports aircraft and light rotorcraft,
3. Description of the mechanisms of energy savings, and
4. Analysis of the scaling of the energy savings with mission and technology parameters, and definition of the key enabling improvements in electrical component technology.

1.3 Thesis Outline

The remaining chapters are organized as follows. In Chapter 2, the modeling approach, including the optimization framework used and detailed descriptions of the

propulsion system, aircraft, rotorcraft, and mission models are described. In Chapter 3, results for aircraft designs with different mission and technology assumptions are presented, including an analysis of the energy savings for off-design missions and the mechanisms of energy savings with the hybrid propulsion system. In Chapter 4, a sensitivity analysis of the hybrid-electric design is presented, and the scaling of the hybridization benefit to the design mission and electrical technology parameters to which performance is most sensitive are analyzed. In Chapter 5, preliminary results for the application of parallel hybrid electric propulsion for rotorcraft are presented. Chapter 6 provides a summary, conclusions, and suggestions for future work.

Chapter 2

Modeling Approach

To assess the performance of parallel hybrid aircraft propulsion systems, we develop an optimization model for conceptual design and performance analysis of conventional and hybrid aircraft. This chapter describes the modeling approach, including the optimization framework used, the choice of objective function, and the constraints that form models for aircraft, rotorcraft, propulsion system, and mission design. The models were developed using GPkit, a Python package for setting up and solving geometric program optimization models. The aircraft optimization model, summarized in section 2.7, is applied in Chapters 3-5 to assess the potential benefits of parallel hybrid electric propulsion and to provide insight into the mechanism of those benefits.

2.1 Geometric Programming

The propulsion system is modeled in the context of an aircraft conceptual design optimization, which is solved using geometric programming techniques. A *Geometric Program* (GP), a non-linear optimization problem of the form,

$$\begin{aligned} &\text{minimize} && g_0(\mathbf{x}) \\ &\text{subject to} && f_i(\mathbf{x}) = 1,\ i = 1, \dots m \\ & && g_j(\mathbf{x}) \leq 1, j = 1, \dots n, \end{aligned} \tag{1}$$

where $\mathbf{x}$ is a vector of design variables, and the objective function and constraints are composed of *monomials*, $f(\mathbf{x})$, and *posynomials*, $g(\mathbf{x})$, of the form,

$$f(\mathbf{x}) = c x_1^{a_1} x_2^{a_2} \dots x_n^{a_n}, \qquad a \in \mathbb{R}, \tag{2}$$

$$g(\mathbf{x}) = \sum_{k=1}^{K} c_k x_1^{a_{1,k}} x_2^{a_{2,k}} \dots x_n^{a_{n,k}}, \qquad a, c \in \mathbb{R}, c > 0. \tag{3}$$

To illustrate, vehicle design can be represented as a geometric program formulation; consider the following optimization model for wing aerodynamic performance:

$$\begin{aligned} &\text{minimize} && D \\ &\text{by varying} && \mathbf{x} = [b, c, S_{\text{ref}}, \text{AR}, L, D, C_L, C_D] \\ &\text{subject to} && D = q C_D S_{\text{ref}}, \\ & && C_D \geq C_f \frac{S_{\text{wet}}}{S_{\text{ref}}} + \frac{C_L^2}{\pi(\text{AR}) e}, \\ & && S_{\text{ref}} = bc, \\ & && \text{AR} = \frac{b^2}{S_{\text{ref}}}, \\ & && L = q C_L S_{\text{ref}}, \\ & && L \geq W, \\ & && b \leq b_{\max}. \end{aligned} \tag{4}$$

Assuming dynamic pressure, q, wetted area, S_{wet}, skin friction coefficient, C_f, Oswald efficiency, e, maximum span, $b_{\max}$, and weight, W, are specified as constant

parameters, solution of (4) will produce an optimized geometry $(b, c, \mathrm{AR}, S_{\mathrm{ref}})$ and performance (C_L, C_D) what minimizes drag, D, while producing the required lift. The first constraint is a monomial equality constraint that can be expressed in the form given in (1) by dividing both sides of the equation by D. The second constraint is a posynomial inequality constraint. At the optimal solution, the constraint should be active: the drag coefficient should be *equal to* the sum of the two terms on the right side of the equation, representing the zero-lift drag and the drag due to lift. Minimizing the drag force, however, implies setting a lower bound on C_D is sufficient because the value that minimizes the drag force will occur at this lower bound. In other words, the minimization of the drag force always puts a "downward pressure" on the drag coefficient, so it will be pushed to its lower bound, and the inequality constraint will be active. This principle is frequently used when creating models to ensure posynomial constraints satisfy the form of Equation (3).

GPs can be converted into convex optimization problems through a logarithmic transformation, and they may thus be solved taking advantage of features of convex problems: numerical solution yields either a global optimum or a proof of infeasibility, and can be achieved using existing solvers that are fast and provide converged solutions regardless of the initial guess [24]. The restrictions on the form of the constraints make geometric programming well-suited for conceptual design models, where models such as physics-based scaling or empirical data fits can be expressed as monomial or posynomial constraints. When one or more constraints cannot be made GP, a *Signomial Program* (SP), where the coefficients, c_k, in posynomial constraints (Equation (3)) are permitted to be negative, can still be solved using iterative solution of locally GP approximations,

although this comes at the cost of the guarantee of global optimality and robustness of the solution methods, which apply only to GPs. In practice, however, models with a small number of SP constraints and appropriate initial guesses for the associated design variables may be solved as quickly and reliably as GPs. The models described below are implemented in GPkit, a Python package for defining and solving GPs and SPs, which has been applied to aircraft and propulsion system conceptual design [25], both for conventional architectures and novel electrified aircraft concepts, as discussed in Section 1.1.4. For the purposes of this study, use of geometric programming enabled detailed analysis of off-design performance and design space exploration through variation of relevant mission and technology parameters with low computational cost.

2.2 Objective Function: Total Mission Energy

The optimization framework requires definition of an objective function to be minimized and we use total mission energy consumption, E,

$$g_0(x) = E \geq m_{\text{batt}}\text{BSE} + m_{\text{fuel}}h_{\text{fuel}}, \tag{5}$$

where m_{batt} and m_{fuel} are the battery and fuel mass required for the mission, which are design variables, and BSE and h_{fuel} = 43 MJ/kg are the effective battery specific energy and specific energy of jet fuel, which are constant parameters in the optimization. The right-hand side of Equation (5) is another example of a posynomial inequality constraint; at the optimal design point, the inequality constraint is active, behaving effectively like an equality constraint.

Other objective functions of interest, such as CO_2 emissions or energy related operating costs, could also be considered by weighting the two terms on the right-hand side of Equation (4) differently. Two factors, however, make mission energy an appropriate objective function in the current context. First, uncertainty in future fuel and energy prices, regulations, and carbon intensity of the electrical energy generation make it difficult to assign appropriate weights with any confidence. Second, the results will show that the low specific energy of the electrical energy storage results in designs where it accounts for less than 1% of the overall mission energy; the benefit of electrification is not replacing fuel with batteries, but rather using a small amount of electrical energy to improve the efficiency of the fuel-burning system. Because the cost and carbon intensity of both sources of energy are comparable [8], total mission energy also provides a useful surrogate measure of the impact on economic and environmental metrics.

2.3 Propulsion System Component Sizing and Performance

2.3.1 Parallel Hybrid Propulsion System

The parallel hybrid-electric turboprop (PHET) propulsion system configuration model is depicted in Figure 2-1. It consists of a gas turbine engine and a battery-powered electric drivetrain, including power electronics and an electric motor. The turbine and motor provide shaft power to the propeller through a gearbox. The propulsion system model consists of models describing each component along with constraints connecting them.

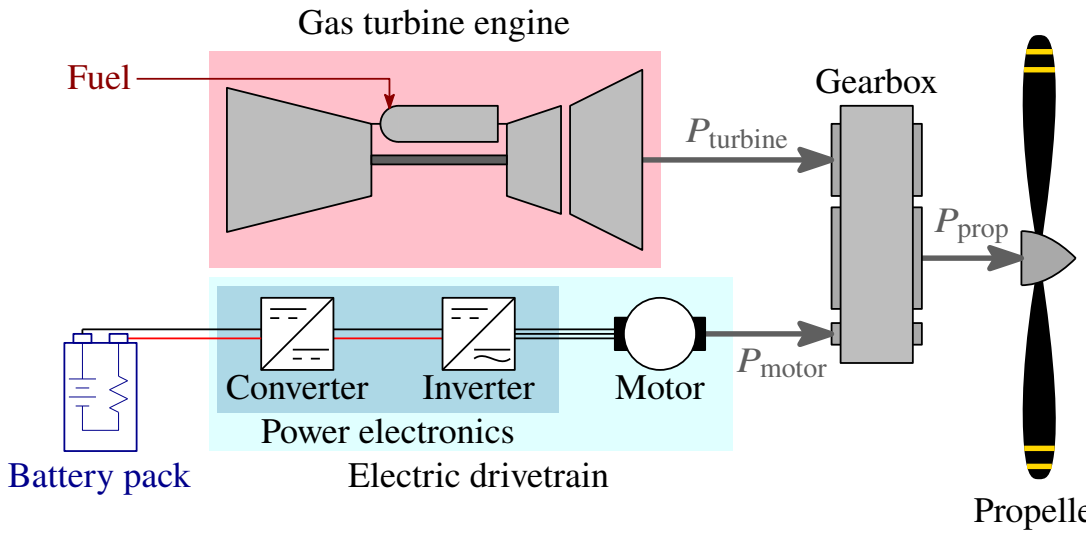

Figure **2-1**: Parallel hybrid electric turboprop propulsion system configuration model schematic.

The engine mass is built up from the masses of its components, each of which has a mass sizing model of its own described below,

$$m_{\text{eng}} \geq m_{\text{gg}} + m_{\text{gb}} + m_{\text{mot}} + m_{\text{pe}} + m_{\text{cable}} + m_{\text{prop}}. \tag{6}$$

The flow of power through the propulsion system is constrained at the inputs and outputs of the gearbox and cable. The shaft power of the motor and gas turbine are combined and output to the propeller, with some losses from the gearbox. Due to the structure of the parallel hybrid propulsion system, this constraint is inherently signomial,

$$P_{\text{shaft}} + P_{\text{mot}} \geq P_{\text{gb,in}}, \tag{7}$$

$$P_{\text{gb,out}} \geq P_{\text{prop}}. \tag{8}$$

For the conventional aircraft model, the masses and power of electrical components in the above equations are zero. For the parallel hybrid electric model, power passes through the electrical components,

$$V_{\text{batt}} = V_{\text{cable}}, \tag{9}$$

$$I_{\text{batt}} N_{\text{eng}} \geq I_{\text{cable}}, \tag{10}$$

$$P_{\text{out,cable}} \geq P_{\text{in,pe}}, \tag{11}$$

$$P_{\text{out,pe}} \geq P_{\text{in,mot}}. \tag{12}$$

The cable receives power from the battery in the form of electrical current at the output voltage of the battery.

The thrust produced by the engine is the sum of the thrust force of the propeller and the exhaust thrust of the gas turbine engine:

$$F_{\text{net}} \leq F_{\text{prop}} + \dot{m}_{\text{air}}(u_8 - V). \tag{13}$$

Equation (13) is one of a few relations in the model that cannot be expressed as a GP monomial or posynomial constraint, meaning the overall model will be an SP.

2.3.2 Gas Turbine Engine

The gas turbine engine is sized based on a *cube-squared* scaling with engine inlet area,

$$m_{\text{gg}} \geq \left(\frac{m}{A}\right)_{\text{gg}} A_2^{3/2}. \tag{14}$$

Implicit in Equation (14) is an assumption that the mass of the engine, m_{gg}, scales approximately with the inlet diameter cubed, and the inlet area, A_2, scales with the diameter squared. The coefficient, $\left(\frac{m}{A}\right)_{\text{gg}}$, was tuned to accurately estimate the weight of the PW120 engine that powers the DHC-8-100 aircraft in the baseline model described in Chapter 3. The inlet area is constrained by a maximum corrected flow constraint,

described below, and Equation (14) thus essentially models a cube-squared scaling with maximum corrected flow.

The gas turbine engine performance is described using a Brayton cycle with constant component efficiencies. The model relates the fuel and air flow to the turbine shaft power and core thrust at a given operating point. The engine is comprised of a compressor, combustor, core turbine, power turbine, and nozzle. The aero-thermodynamic state changes through each component are modeled based on cycle temperature and pressure ratios and component matching described below. Figure 2-2 shows an example of the stagnation temperature versus the relative entropy for a typical engine cycle.

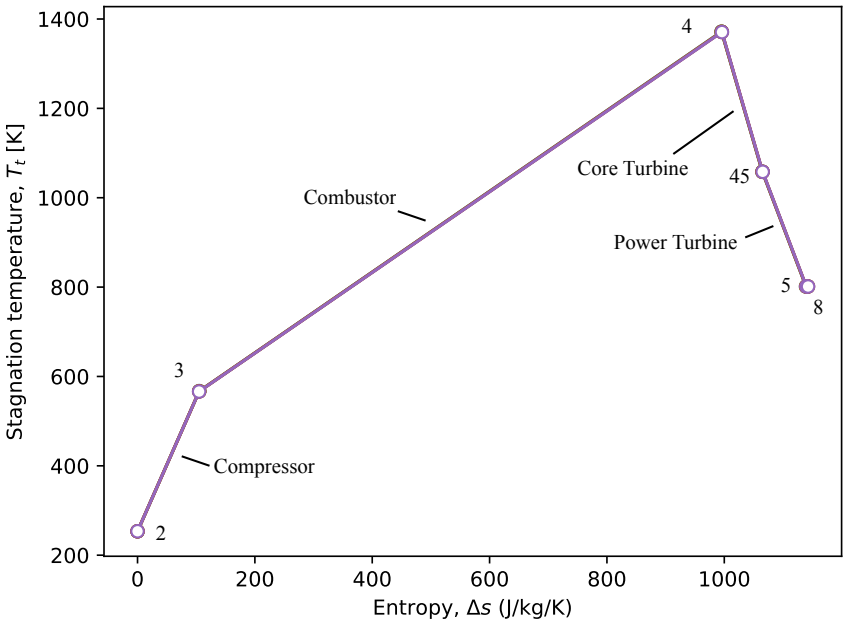

Figure **2-2**: Example stagnation temperature versus relative entropy of the gas turbine engine cycle.

Compressor:

The compressor inlet stagnation quantities are assumed to be equal to the free stream stagnation conditions, which are specified as constant parameters in the optimization. The inlet corrected flow per unit area, D_2, is bounded above by a constant corresponding to a maximum compressor inlet Mach number,

$$D_2 = \frac{\dot{m}_{\text{air}}}{A_2 p_{t2}} \sqrt{\frac{R_{\text{gas}} T_{t2}}{\gamma_c}} \leq D_{2,\max}\,, \tag{15}$$

where R_{gas} is the specific gas constant of air and γ_c is the ratio of specific heats of air in the compressor, both constants. The stagnation temperature and pressure both increase across the compressor, and their ratios of outlet (Station 3) to inlet (Station 2) values are related through the adiabatic compressor efficiency η_c. The stagnation pressure ratio, π_c, is limited by a specified upper bound, $\pi_{\text{c,max}}$, and maximum compressor exit temperature, $T_{t3,\max}$,

$$\frac{T_{t3}}{T_{t2}} = \pi_c{}^{(\gamma_c - 1)/\gamma_c \eta_c}, \tag{16}$$

$$\pi_c = \frac{p_{t3}}{p_{t2}} \leq \pi_{\text{c,max}}\,, \tag{17}$$

$$T_{t3} \leq T_{t3,\max}\,. \tag{18}$$

Combustor:

In the burner, heat from the combustion of fuel is added to the flow. The stagnation temperature rise is based on the specific heat of air, which varies slightly due

to the high temperature in the burner, while the heat released by the combusting fuel is the product of the fuel burn rate, $\dot{m}_{\text{fuel}}$, and specific energy of jet fuel, h_{fuel}:

$$\dot{m}_{\text{fuel}} h_{\text{fuel}} \geq \dot{m}_{\text{air}} R_{\text{gas}} \left(\frac{\gamma_t T_{t4}}{\gamma_t - 1} - \frac{\gamma_c T_{t3}}{\gamma_c - 1} \right), \tag{19}$$

where γ_t is the ratio of specific heats in the turbine, a constant. The losses in the burner are represented by the pressure ratio across the burner, π_b. The stagnation temperature at the burner exit, T_{t4}, is limited by a specified maximum turbine inlet temperature,

$$\pi_b = \frac{p_{t4}}{p_{t3}}, \tag{20}$$

$$T_4 \leq T_{4,\text{max}}. \tag{21}$$

Core Turbine:

The core turbine provides power for the compressor. The flow is assumed to be choked at the turbine nozzle throat, denoted as Station 41, and the corrected flow per unit area, D_{41}, is fixed at the sonic value,

$$D_{41} = \frac{\dot{m}_{\text{air}}}{A_{41} p_{t4}} \sqrt{\frac{R_{\text{gas}} T_{t4}}{\gamma_t}}. \tag{22}$$

Both pressure and temperature decrease across the turbine. Conservation of energy requires the stagnation enthalpy increase in the compressor to be equal to the enthalpy drop in the turbine; this is approximated by equating the magnitude of the stagnation temperature change across the two components,

$$T_{t4} - T_{t45} \geq T_{t3} - T_{t2}. \tag{23}$$

Similar to in the compressor model, the pressure ratio is related to the temperature ratio through a specified turbine adiabatic efficiency, η_t,

$$\frac{T_{t4}}{T_{t45}} = \left(\frac{p_{t4}}{p_{t45}}\right)^{(\gamma_t - 1)/\gamma_t \eta_t}. \tag{24}$$

Power Turbine:

The power turbine produces the shaft power that is output to the gearbox and used to turn the propeller. The decrease in the temperature of the flow is related to the shaft power produced by the specific heat of the air and the mass flow through the turbine,

$$\dot{m}_{\text{air}} R_{gas} \frac{\gamma_c}{\gamma_c - 1}(T_{t5} - T_{t45}) \geq P_{shaft}. \tag{25}$$

The temperature and pressure ratios across the power turbine are related through the turbine adiabatic efficiency, η_t,

$$\frac{T_{t45}}{T_{t5}} = \left(\frac{p_{t45}}{p_{t5}}\right)^{(\gamma_t - 1)/\gamma_t \eta_t}. \tag{26}$$

Nozzle:

Lastly, the turbine exit flow is accelerated through the nozzle. The stagnation temperature of the flow is constant, and nozzle losses are characterized by nozzle pressure ratio, π_n,

$$\pi_n = \frac{p_{t8}}{p_{t5}}. \tag{27}$$

To find the exhaust velocity, the static temperature and Mach number are needed. The Mach number at the nozzle exit can be determined using the corrected flow function, and isentropic relations can be used to relate the stagnation and static quantities at the nozzle exit:

$$u_8 = M_8\sqrt{\gamma_t R_{\text{gas}} T_8}\,, \tag{28}$$

$$D_8 \leq \frac{M_8}{\left(1 - \frac{\gamma - 1}{2} M_8^2\right)^{(\gamma_t+1)/2(\gamma_t-1)}}, \tag{29}$$

$$\left(\frac{p_{t8}}{p_8}\right)^{(\gamma_t-1)/\gamma_t} = \left(\frac{M_8}{D_8}\right)^{2(\gamma_t-1)/(\gamma_t+1)}, \tag{30}$$

$$\frac{p_{t8}}{p_8} = \left(\frac{T_{t8}}{T_8}\right)^{\gamma_t/(\gamma_t-1)}. \tag{31}$$

Idle Power Constraint:

To model engine idle power, the corrected shaft power, P^*_{shaft}, is limited to no less than half the maximum rated power, P^*_{max}. The corrected power is defined using the ratios of stagnation temperature and pressure to their sea level static values:

$$\theta = \frac{T_t}{288.15\ \mathrm{K}}, \tag{32}$$

$$\delta = \frac{p_t}{101325\ \mathrm{Pa}}, \tag{33}$$

$$P^*_{\mathrm{shaft}} = \frac{P_{\mathrm{shaft}}}{\delta\sqrt{\theta}}, \tag{34}$$

$$P^*_{\mathrm{max}} \geq P^*_{\mathrm{shaft}} \geq \frac{P^*_{\mathrm{max}}}{2}. \tag{35}$$

Cycle Performance:

The description of gas turbine engine performance captures the changes in cycle thermal efficiency with changes in operating condition. As the corrected power increases, the thermal efficiency increases. This relationship is shown in Figure 2-3, including operating points from a representative regional turboprop mission.

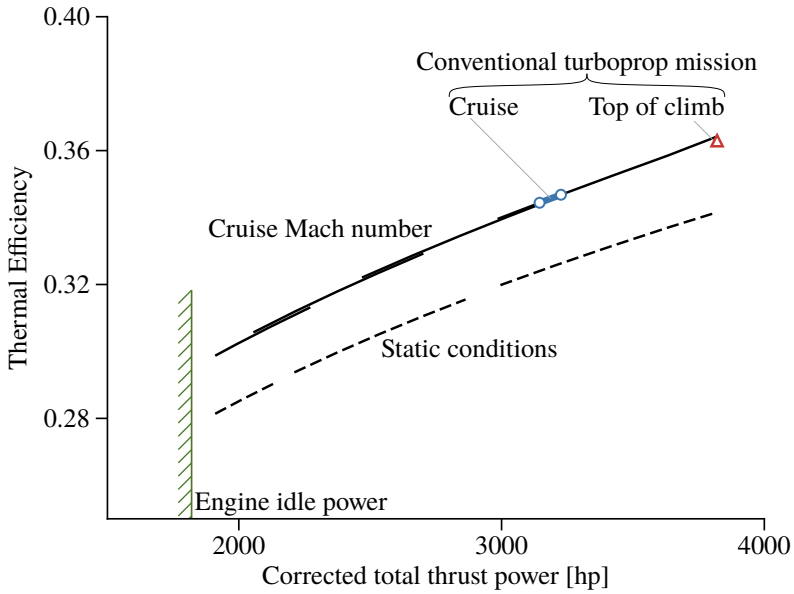

Figure **2-3**: Gas turbine engine thermal efficiency vs. corrected total thrust power at static conditions and cruise Mach number, including representative regional turboprop cruise and climb operating points

2.3.3 Gearbox

The mass of the gearbox, m_{gb}, is estimated using the NDARC AFDD00 weight model [26], based on power-law scaling with maximum gearbox power, P_{max}, and shaft speeds, Ω_{eng} and Ω_{prop},:

$$m_{\mathrm{gb}} \geq 95.7634\, N_{\mathrm{prop}}^{0.38553} P_{\mathrm{max}}^{0.78137} \frac{\Omega_{\mathrm{eng}}^{0.09899}}{\Omega_{\mathrm{prop}}^{0.80686}}. \tag{36}$$

Losses in the gearbox were modeled using a constant efficiency, assumed to be $\eta_{\mathrm{gb}} = 99\%$. To express the gearbox performance with geometric programming constraints, the *inefficiency*, $\left(1 - \eta_{\mathrm{gb}}\right)$, was specified as a constant design parameter,

$$P_{\mathrm{gb,in}} \geq P_{\mathrm{gb,out}} + Q_{\mathrm{gb}}, \tag{37}$$

$$Q_{\mathrm{gb}} = \left(1 - \eta_{\mathrm{gb}}\right) P_{\mathrm{gb,in}}. \tag{38}$$

In Equations (37) and (38), Q_{gb} is the power lost as heat in the gearbox.

2.3.4 Propeller

The propeller mass, m_{prop}, is assumed to scale with its diameter, d_{prop}, cubed. It is also assumed to have a constant hub-to-tip ratio which increases the diameter, and therefore the mass, required to achieve a given disk area, A_{prop},

$$m_{\mathrm{prop}} \geq \left(\frac{m}{d^3}\right)_{\mathrm{prop}} d_{\mathrm{prop}}^3 \,, \tag{39}$$

$$r_{\mathrm{tip}} = d_{\mathrm{prop}}/2 \,, \tag{40}$$

$$A_{\mathrm{prop}} + \pi r_{\mathrm{hub}}^2 \leq \pi r_{\mathrm{tip}}^2 \,. \tag{41}$$

As with the gas turbine engine, the scaling coefficient, $\left(\frac{m}{d^3}\right)_{\mathrm{prop}}$, was tuned to match the mass of the DHC-8-100 propeller in the baseline model.

The propeller thrust and power are related using momentum theory which can be expressed using GP constraints. A constant figure of merit, FOM, is included to account for viscous and induced losses in the propulsive streamtube,

$$\frac{1}{2}\rho u_e^2 A_{\text{prop}} \geq \frac{1}{2}\rho u_0^2 A_{\text{prop}} + F_{\text{prop}}, \tag{42}$$

$$P_{\text{prop}} \geq \frac{F(u_e + u_0)}{2(\text{FOM})}, \tag{43}$$

$$\eta_p = \frac{u_0 F_{\text{prop}}}{P_{\text{prop}}}. \tag{44}$$

2.3.5 Turboprop Design Variables and Parameters

Tables 2-1, 2-2, and 2-3 list the symbols and descriptions of the design variables and parameters used in the constraints for the propulsion system, gas turbine engine, gearbox, and propeller. For a given design optimization, the sizing variables are constant while the performance variables vary over many discrete operating points.

Table **2-1**: Propulsion system component sizing design variables

	Symbol	Description
Engine	m_{eng}	Engine mass
Gas Turbine Engine	m_{gg}	Gas generator mass
	A_2	Compressor inlet area
	A_4	Turbine inlet nozzle throat area
	A_8	Nozzle exit area
	P^*_{max}	Maximum corrected power turbine shaft power
Gearbox	m_{gb}	Gearbox mass
	P_{max}	Maximum output power
Propeller	m_{prop}	Propeller mass
	A_{prop}	Propeller area
	r_{hub}	Propeller hub radius
	r_{tip}	Propeller tip radius

Table **2-2**: Propulsion system component performance design variables

	Symbol	Description
Engine	F_{net}	Total force produced by propulsion system
Gas Turbine Engine	$\dot{m}_{\text{air}}$	Air mass flow rate
	$\dot{m}_{\text{fuel}}$	Fuel mass flow rate
	T_{ti}	Stagnation temperature at station i (see Figure 2-2)
	p_{ti}	Stagnation pressure at station i
	D_i	Corrected flow per unit area at station i
	π_c	Compressor pressure ratio
	M_8	Nozzle exit Mach number
	u_8	Nozzle exit flow velocity
	P_{shaft}	Power turbine shaft power
	P^*_{shaft}	Corrected power turbine shaft power
Gearbox	$P_{\text{gb,in}}$	Gearbox input power
	$P_{\text{gb,out}}$	Gearbox output power
	Q_{gb}	Gearbox heat rejected
Propeller	F_{prop}	Propeller thrust
	P_{prop}	Propeller shaft power
	u_e	Propeller jet velocity
	η_p	Propulsive efficiency
	ρ	Air density
	u_0	Free stream velocity

Table **2-3**: Propulsion system component constant parameters

	Symbol	Description	Value
Gas Turbine Engine	$\left(\frac{m}{A}\right)_{\text{gg}}$	Gas turbine engine mass scaling factor	19,751 kg/m^3
	h_{fuel}	Specific energy of jet fuel	43 MJ/kg
	$\pi_{\text{c,max}}$	Max compressor pressure ratio	15
	$D_{2,\text{max}}$	Max corrected flow per unit area	0.3625
	$T_{t3,\text{max}}$	Max compressor exit stagnation temperature	1400 K
	$T_{t4,\text{max}}$	Max turbine inlet stagnation temperature	1400 K
	π_b	Burner pressure ratio	0.99
	π_n	Nozzle pressure ratio	0.99
	Ω_{eng}	Power turbine shaft speed	28900 rpm
	η_c	Compressor efficiency	0.9
	η_t	Turbine efficiency	0.9
	γ_c	Ratio of specific heats of air in compressor	1.4
	γ_t	Ratio of specific heats of air in turbine	1.35
	R_{gas}	Specific gas constant of air	287 J/kg/K
Gearbox	N_{prop}	Number of propellers connected to gearbox	1
	η_{gb}	Gearbox efficiency	0.99
	Ω_{in}	Input shaft speed	28900 rpm
	Ω_{out}	Output shaft speed	1200 rpm
Propeller	$\left(\frac{m}{d^3}\right)_{\text{prop}}$	Propeller mass scaling factor	0.143 lb/ft^3
	d_{prop}	Propeller diameter	13 ft
	$\frac{r_{\text{hub}}}{\text{r}_{tip}}$	Propeller hub-to-tip ratio	0.17
	FOM	Propeller figure of merit	0.80
	Ω_{prop}	Propeller angular speed	1200 rpm

2.4 Electrical Component Sizing and Performance

The parallel hybrid electric propulsion system includes a motor, power electronics, cabling, and a battery. The mass scaling and performance parameters used in the models for these components depend on the technology level of the components.

Values for state-of-the-art technology and projected technology from about 2035 are included in Table 2-6.

2.4.1 Electric Motor

An empirical power law relation with maximum torque, $T_{\max}$, from [27] was used to model the weight of the motor, m_{mot},

$$m_{\text{mot}} = k_{\text{mot}} T_{\max}^{0.75}. \tag{45}$$

An internal resistance model was used to model the losses in the motor. As in the gearbox, losses are modeled by Q_{mot}, the power lost to heat in the motor with internal resistance R_{mot}. The voltage of the motor, V_{mot}, is equal to the output voltage of the battery, while the motor current, I_{mot}, is determined by the electrical power required:

$$P_{\text{mot,elec}} \geq P_{\text{mot,shaft}} + Q_{\text{mot}}\,, \tag{46}$$

$$Q_{\text{mot}} = I_{\text{mot}}^2 R_{\text{mot}}, \tag{47}$$

$$P_{\text{mot,elec}} = I_{\text{mot}} V_{\text{mot}}, \tag{48}$$

$$\frac{P_{\text{mot,shaft}}}{\Omega_{\text{mot}}} = T \leq T_{\max}. \tag{49}$$

2.4.2 Power Electronics

To model the power electronics, a constant specific power, $\left(\frac{P}{m}\right)_{\text{PE}}$, is used to determine the mass, and a constant efficiency, η_{PE}, is used to determine the lost power,

Q_{PE}. To keep the efficiency constraints GP, the inefficiency, $(1-\eta_{\mathrm{PE}})$, is specified as a parameter in the optimization model:

$$m_{\mathrm{PE}} \geq P_{\mathrm{PE,max}} \left(\frac{P}{m}\right)_{\mathrm{PE}}, \tag{50}$$

$$P_{\mathrm{PE,in}} \geq P_{\mathrm{PE,out}} + Q_{\mathrm{PE}}, \tag{51}$$

$$Q_{\mathrm{PE}} \geq (1-\eta_{\mathrm{PE}}) P_{\mathrm{PE,in}}. \tag{52}$$

2.4.3 Cable

The cable sizing and performance models are based on a Litz wire insulated by a dielectric [4]. The cable is 10 meters long per engine, approximately half of the wingspan. The linear mass density and resistance per unit length of the cable is determined by the power through the cable; for the state-of-the-art clean-sheet hybrid design, the mass are resistance per unit length are 0.23 kg/m and 0.38 mΩ/m, respectively. The cable does not significantly affect the propulsion system performance due to its light weight and low resistance.

2.4.4 Battery

The battery is sized based on a specified battery specific energy, BSE, and depth of discharge, $\mathrm{DOD}_{\mathrm{max}}$. In this study, the depth of discharge was set to 100%, making BSE an *effective pack-level* specific energy,

$$m_{\text{batt}} \geq \frac{E_{\text{batt}}}{\text{BSE} \cdot \text{DOD}_{\text{max}}}. \quad (53)$$

An internal resistance model was used for the battery performance. The internal resistance of the battery can be determined by the maximum discharge rate, or C-rate. The C-rate is defined as the rate of discharge divided by the capacity. For example, a battery with a maximum C-rate of 2 takes at least half an hour to discharge completely. The internal resistance of the battery, R_{batt} can be determined as a function of the maximum C-rate based on a circuit model consisting of a voltage source, $\mathcal{E}$, and resistance, R_{batt}, in series [4]:

$$R_{\text{batt}} = \frac{\mathcal{E}^2}{4E_{\text{batt}}C_{\text{max}}}, \quad (54)$$

$$\mathcal{E} \geq V_{\text{batt}} + I_{\text{batt}}R_{\text{batt}}, \quad (55)$$

$$\dot{E}_{\text{batt}} = \mathcal{E}I_{\text{batt}}. \quad (56)$$

2.4.5 Electrical Component Design Variables and Parameters

Tables 2-4, 2-5, and 2-6 list the symbols and descriptions of the design variables and parameters used in the constraints for the motor, power electronics, cable, and battery. The state-of-the-art and projected technology assumptions are derived from [2].

Table **2-4**: Electrical component sizing design variables

	Symbol	Description
Motor	m_{mot}	Motor mass
	T_{max}	Motor maximum torque
Power Electronics	m_{PE}	Power electronics mass
	$P_{\mathrm{PE,max}}$	Power electronics maximum input power
Cable	m_{cable}	Cable mass
	R_{cable}	Cable resistance
Battery	m_{batt}	Battery mass
	E_{batt}	Effective battery energy capacity
	R_{batt}	Battery internal resistance

Table **2-5**: Electrical component performance design variables

	Symbol	Description
Motor	$P_{\mathrm{mot,shaft}}$	Motor output shaft power
	$P_{\mathrm{mot,elec}}$	Motor input electrical power
	Q_{mot}	Motor heat rejected
	T_{mot}	Motor torque
	V_{mot}	Motor voltage
	I_{mot}	Motor current
Power Electronics	$P_{\mathrm{PE,in}}$	Power electronics input power
	$P_{\mathrm{PE,out}}$	Power electronics output power
	Q_{PE}	Power electronics heat rejected
Cable	$V_{\mathrm{cable,in}}$	Cable input voltage
	$V_{\mathrm{cable,out}}$	Cable output voltage
	I_{cable}	Cable current
Battery	$\dot{E}_{\mathrm{batt}}$	Battery discharge rate
	V_{batt}	Battery operating voltage
	I_{batt}	Battery current

Table **2-6**: Electrical component constant parameters

	Symbol	Description	State-of-the-art	Projected
Motor	k_{mot}	Motor mass scaling factor	0.33	0.081
	R_{mot}	Motor internal resistance	50 mΩ	10 mΩ
	Ω_{mot}	Motor speed	28900 rpm	
Power Electronics	$\left(\frac{P}{m}\right)_{\text{PE}}$	Power electronics specific power	2.2 kW/kg	9 kW/kg
	η_{PE}	Power electronics efficiency	0.95	0.975
Cable	ℓ_{cable}	Cable length	30 ft	
	$\left(\frac{m}{\ell}\right)_{\text{cable}}$	Cable mass per unit length	0.23 kg/m	
	$\left(\frac{R}{\ell}\right)_{\text{cable}}$	Cable resistance per unit length	0.38 mΩ/m	
Battery	BSE	Battery specific energy	250 Wh/kg	600 Wh/kg
	C_{max}	Battery maximum discharge rate	10 1/hr	
	DOD_{max}	Battery depth of discharge	100%	
	$\mathcal{E}_{\text{batt}}$	Battery internal voltage	540 V	

2.5 Aircraft Sizing and Performance

2.5.1 Fixed Wing Aircraft

The total mass of the aircraft is comprised of the aircraft operating empty weight, m_{empty}, including the battery and propulsion system weights, m_{batt} and $N_{\text{eng}}m_{\text{eng}}$, respectively, and the payload and fuel weight, which will depend on the mission. The empty weight excluding the battery and propulsion systems is assumed to scale with the maximum allowable takeoff weight, m_{MTO}, with empty weight fraction, f_{empty}:

$$m_{\text{empty}} \geq m_{\text{MTO}} f_{\text{empty}} + N_{\text{eng}} m_{\text{eng}} + m_{\text{batt}}. \tag{57}$$

Power-law scaling relationships for empty weight fraction, f_{empty}, as a function of maximum takeoff weight, m_{MTO}, and maximum fuel capacity, m_{MF}, as a function of the wingspan, b_{wing}, and aspect ratio, AR_{wing}, were developed based on data from 12 regional turboprop aircraft:

$$f_{\text{empty}} \geq 5.1792 \left(m_{\text{MTO}}\ (\text{lb})\right)^{-0.209}, \tag{58}$$

$$\frac{\left(b_{\text{wing}}(\text{ft})\right)^3}{\left(\text{AR}_{\text{wing}}\right)^2} = 427.87 \left(m_{\text{MF}}(\text{lb})\right)^{0.2581}. \tag{59}$$

The performance of the aircraft is characterized at each point in the mission using a zero-lift drag based on skin friction coefficient, $C_{f,e}$, and reference and wetted areas, S_{ref} and S_{wet} and induced drag based on the lift coefficient, C_L, wing aspect ratio, and Oswald efficiency factor, e [28]. The drag margin, $\mathcal{M}_D$, is a tuning parameter used to tune the drag model to closely match reference aircraft performance data:

$$C_D \geq C_{D,0} + C_{D,i}, \tag{60}$$

$$\frac{C_{D,0}}{\mathcal{M}_D} \geq C_{f,e} \frac{S_{\text{ref}}}{S_{\text{wet}}}, \tag{61}$$

$$\frac{C_{D,i}}{\mathcal{M}_D} \geq \frac{C_L^2}{\pi\left(\text{AR}_{\text{wing}}\right)e}. \tag{62}$$

2.5.2 Rotorcraft

The rotorcraft model requires a fixed fuselage weight as an input parameter. This weight does not include the weight of the engine, as it is modeled separately. The empty weight of the rotorcraft is the sum of all of the fuselage, engine, and battery weights. The main rotor area is calculated from the rotor radius:

$$m_{\text{empty}} \geq m_{\text{fuse}} + m_{\text{eng}} + m_{\text{batt}}, \tag{63}$$

$$A_{\text{mr}} = \pi R_{\text{mr}}^2, \tag{64}$$

and the rotor angular speed is defined as the rotor tip speed divided by the rotor radius:

$$\Omega_{\text{mr}} = \frac{v_{\text{tip}}}{R_{\text{mr}}}. \tag{65}$$

To model the power required to be produced by the rotor, a power build up is used. The total power required, P_{mr}, is the sum of the induced power, P_i, profile power, P_o, and parasite power, P_p, of the rotorcraft:

$$P_{\text{mr}} = P_i + P_o + P_p. \tag{66}$$

In hover, the majority of the rotor power comes from the induced power, which is a function of the main rotor thrust and the induced velocity of the flow through the rotor. During hover, the main rotor thrust, T_{mr}, is equal to the weight of the rotorcraft, W_{ave}, plus a 10% margin such that the rotorcraft is capable of climbing to a hover and maneuvering:

$$T_{\text{mr}} \geq 1.1 W_{\text{ave}}. \tag{67}$$

The induced velocity of flow through the rotor, v_i, is related to the thrust using momentum theory and used to calculate the induced power [29]:

$$v_i = \sqrt{\frac{T_{\text{mr}}}{2A_{\text{mr}}\rho}}, \tag{68}$$

$$P_i \geq T_{\text{mr}} v_i. \tag{69}$$

The profile power is a result of the profile drag on the rotor blades, and obeys the same relationship during hover and forward flight. Blade element theory yields the following equation for the profile power coefficient of a blade with constant chord and constant drag coefficient, C_{d_o}, which can be used to calculate the profile power:

$$C_{P_o} = \frac{\sigma C_{d_o}}{8}, \tag{70}$$

$$P_o \geq C_{P_o} \rho A_{\text{mr}} v_{tip}^3. \tag{71}$$

During hover, the parasite power is zero.

In forward flight, the thrust is the resultant force of the weight and drag of the rotorcraft:

$$T_{\text{mr}}^2 \geq (m_{\text{ave}} g)^2 + D^2, \tag{72}$$

where the drag force, D, on the aircraft scales proportionally to the cruise velocity, v_{cruise}, squared with a scaling factor, k:

$$D \geq k\left(\frac{1}{2}\rho v_{\text{cruise}}^2\right). \tag{73}$$

An approximation of momentum theory valid above very low speeds is used to calculated the induced power as a function of the thrust and cruise speed:

$$P_i \geq \frac{T_{\text{mr}}^2}{2\rho A_{\text{mr}} v_{\text{cruise}}}. \tag{74}$$

The profile power is modeled the same as during cruise, as shown in Equations (70) and (71), resulting in a profile power that is constant with airspeed. Lastly, the parasite power

is the power required to move the rotorcraft through the air against the drag force, D. Since the velocity and drag during hover are zero, the parasite power during hover is zero. In cruise, the parasite power is the product of the drag force and cruise speed:

$$P_p \geq D v_{\text{cruise}} \tag{75}$$

Figure 2-4 shows notional total power and its components versus flight speed curve during cruise.

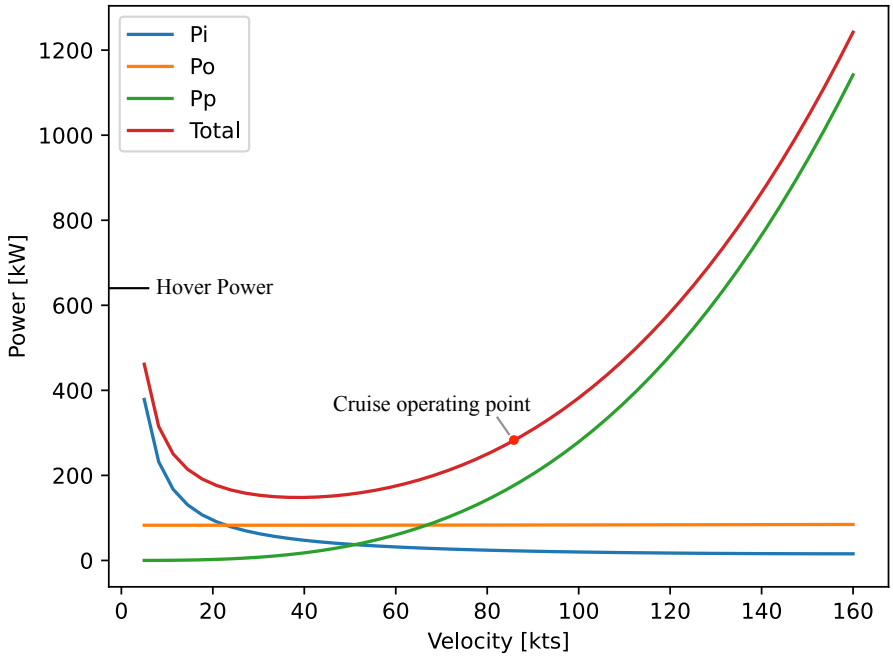

Figure **2-4**: Notional rotorcraft required shaft power versus velocity during forward flight

2.5.3 Aircraft Design Variables and Parameters

Tables 2-7, 2-8, and 2-9 list the symbols and descriptions of the design variables and parameters used in the constraints for fixed-wing aircraft and rotorcraft models.

Sizing parameters are based on the OH-58 Kiowa, but performance parameters are more notional.

Table **2-7**: Aircraft sizing design variables

	Symbol	Description
Aircraft	m_{MTO}	Maximum takeoff mass
	m_{MF}	Maximum fuel mass
	m_{MP}	Maximum payload mass
	m_{empty}	Empty weight including engines and battery
	f_{empty}	Empty weight fraction not including engines or battery
	$\mathrm{AR}_{\mathrm{wing}}$	Wing aspect ratio
	b_{wing}	Wingspan
	S_{ref}	Wing reference area
Rotorcraft	m_{empty}	Rotorcraft weight including engines and battery
	A_{mr}	Main rotor area

Table **2-8**: Aircraft performance design variables

	Symbol	Description
Aircraft	C_D	Drag coefficient
	C_{D_0}	Zero-lift drag coefficient
	C_{D_i}	Induced drag coefficient
	C_L	Lift coefficient
Rotorcraft	D	Rotorcraft drag force
	m_{ave}	Segment average mass
	T_{mr}	Main rotor thrust
	Ω_{mr}	Main rotor speed
	v_i	Rotorcraft induced velocity
	P_i	Main rotor induced power
	C_{P_o}	Profile power coefficient
	P_o	Main rotor profile power
	P_p	Main rotor parasite power
	P_{mr}	Main rotor total power

Table **2-9**: Aircraft constant parameters

	Symbol	Description	Value
Aircraft	$b_{\text{wing,max}}$	Maximum wingspan	85 ft
	C_{f_e}	Equivalent skin friction coefficient	0.0026
	e	Oswald efficiency factor	0.7
	$\mathcal{M}_D$	Drag margin factor	1.2
	N_{eng}	Number of engines	2
	$\frac{S_{\text{wet}}}{S_{\text{ref}}}$	Ratio of wetted to reference wing areas	6
	m_{MTO}	Maximum takeoff mass*	34500 lb
	m_{MF}	Maximum fuel mass*	5678 lb
	m_{MP}	Maximum payload mass*	8408 lb
	S_{ref}	Wing reference area*	585 ft^2
		*These values are not set for clean-sheet designs; instead, these parameters are design variables.	
Rotorcraft	m_{gross}	Maximum gross weight	5500 lb
	m_{fuse}	Rotorcraft empty weight excluding engine, battery	3000 lb
	R_{mr}	Main rotor radius	17.5 ft
	σ	Rotor solidity	0.065
	C_{D_o}	Blade drag coefficient	0.025
	k	Parametric drag scaling factor	0.002 m^2/kg
	v_{cruise}	Rotorcraft cruise true airspeed	85 knots
	v_{tip}	Rotor tip speed	725 ft/s

2.6 Mission Model

2.6.1 Fixed Wing Aircraft

The model simulates the aircraft and propulsion system performance during a parametrically defined mission profile consisting of takeoff, climb, cruise, and descent with allowances for fuel and battery reserves.

Takeoff is modeled as a single point performance constraint as described in [28]; the takeoff distance, ℓ_{TO}, is related to the wing loading, $m_{\mathrm{TO}}g/S_{\mathrm{ref}}$, coefficient of lift at takeoff, $C_{L_{\mathrm{TO}}}$, and thrust to weight ratio, $F_{\mathrm{net}}/m_{\mathrm{TO}}g$:

$$\ell_{\mathrm{TO}} = 40\frac{m_{\mathrm{TO}}g/S_{\mathrm{ref}}}{\sigma C_{L_{\mathrm{TO}}}(F_{\mathrm{net}}/m_{\mathrm{TO}}g)}. \tag{76}$$

The takeoff fuel burn and electrical energy consumption rates are calculated using the propulsion system performance model, and multiplied by the takeoff duration, Δt_{TO}, to determine the fuel and energy used during takeoff.

The remainder of the mission is modeled using the performance models described above in Sections 2.3, 2.4, and 2.5 at discrete states throughout climb, cruise, and descent. These states are connected by segments at which incremental values such as distance traveled, ΔR_{n}, change in velocity, ΔV_{n}, change in altitude, Δh_n, fuel burned, Δm_n, and battery energy used, ΔE_n, are calculated using geometric or algebraic averages of the performance at the beginning and end of the n^{th} segment:

$$\Delta R_{\mathrm{n}} = \Delta t_n\sqrt{V_n V_{n+1}}, \tag{77}$$

$$\Delta V_{\mathrm{n}} = \Delta t_n\sqrt{\dot{V}_n \dot{V}_{n+1}}, \tag{78}$$

$$\Delta h_n = \Delta t_n\sqrt{\dot{h}_n \dot{h}_{n+1}}, \tag{79}$$

$$\Delta m_n = \Delta t_n\, N_{eng}\sqrt{\dot{m}_{fuel,n}\dot{m}_{fuel,n+1}}, \tag{80}$$

$$\Delta E_n = \frac{\Delta t_n}{2}\left(\dot{E}_{\mathrm{batt},n} + \dot{E}_{\mathrm{batt},n+1}\right). \tag{81}$$

Climb is discretized into segments of equal altitude changes; the aircraft flies at a constant indicated airspeed and rate of climb, and the distance traveled during each

segment during climb is a design variable in the optimization. The total time to climb, Δt_{climb}, is constrained to no more than 20 minutes consistent with typical operation of regional transport aircraft:

$$\sum_{\text{climb}} \Delta t \leq \Delta t_{\text{climb}} \leq \Delta t_{\text{climb,max}}. \tag{82}$$

In cruise, the aircraft flies at a constant indicated airspeed at an altitude of 25,000 feet. The mission includes enough fuel for an extended cruise for an additional 45 minutes beyond the design cruise range representative of FAA IFR fuel reserve requirements. During descent, the flight path is constrained to a constant descent angle of 3 degrees, and engine idle power is sufficient to maintain a constant indicated airspeed.

The total range of the mission, R, is the sum of the distance traveled during climb, cruise, and descent, which are themselves sums of the ranges of each subsegment, ΔR_n, in that phase of flight:

$$R_{\text{climb}} + R_{\text{cruise}} + R_{\text{descent}} \geq R, \tag{83}$$

$$\sum_{[\text{phase}]} \Delta R_n \geq R_{[\text{phase}]}. \tag{84}$$

The constraints in Equations (83) and (84) are inherently signomial. Mission fuel and energy consumption are summed similarly over the whole mission, but these constraints can be geometric as the numerical "pressure" on the total fuel, m_{fuel}, and energy consumption, $\Delta E_{\text{mission}}$, of the mission and during each phase is downwards so a lower bound can be used:

$$m_{\text{fuel}} \geq \sum \Delta m_n, \tag{85}$$

$$\Delta E_{\text{mission}} \geq \sum \Delta E_n. \tag{86}$$

where the changes in fuel mass and battery energy during each segment are summed over the whole mission. Fuel is burned throughout the mission such that the takeoff weight, m_{TO}, is the sum of the zero-fuel weight, m_{ZF}, and the fuel burn weight, m_{fuel}:

$$m_{\text{TO}} \geq m_{\text{ZF}} + m_{\text{fuel}}. \tag{87}$$

The net thrust required, $F_{\text{net}}N_{\text{eng}}$, is the sum of the drag, force needed to climb, and force needed to accelerate:

$$F_{\text{net}}N_{\text{eng}} \geq C_D q S_{\text{ref}} + mg\frac{\dot{h}}{V} + m\dot{v} \tag{88}$$

The constraints are the same during each phase of flight with one caveat – during descent, the rate of descent is used rather than the rate of climb since variables must be positive. This means that the climb rate term must be subtracted from both sides of the net force equation, and the resulting descent constraint is a signomial.

2.6.2 Rotorcraft

The rotorcraft mission model is simpler than the fixed-wing aircraft model, and consists of three phases: hover, cruise, and an additional hover phase, and fuel reserve requirements are not taken into consideration. The power requirements during each phase are based on the geometric average of the rotorcraft weight before and after the phase. At the start of a segment, the total rotorcraft weight, m_{total}, is the sum of the empty weight

(including battery and engine), m_{empty}, payload weight, m_{pay}, and fuel weight, m_{fuel}; the total weight at the end of the segment is equal to the total weight at the start of the next segment or, in the case of the final segment, the sum of the empty weight and payload weight with no fuel (fuel reserves are not modeled):

$$m_{\text{gross}} \geq m_{\text{total}} \geq m_{\text{empty}} + m_{\text{pay}} + m_{\text{fuel}}, \tag{89}$$

$$m_{\text{ave}} = \sqrt{m_{\text{start}} m_{\text{end}}}. \tag{90}$$

The mass of fuel burned, Δm_{fuel}, is the product of the fuel mass flow rate of the engine, $\dot{m}_{\text{fuel}}$, and the phase duration, Δt_{seg},

$$\Delta m_{\text{fuel}} \geq \dot{m}_{\text{fuel}} \Delta t_{\text{seg}}. \tag{91}$$

2.6.3 Atmosphere Model

At each operating point throughout the mission, several flow parameters are needed for determining the lift and drag on the aircraft or rotorcraft, as well as influencing the performance of the gas turbine engine and propeller. For these purposes, the *flight state* is defined at each operating point, containing the flow parameters listed in Table 2-10. All of the flow parameters needed, including dynamic pressure, q, density, ρ, and airspeed, V, can be calculated from the Mach number, M, static pressure, p, stagnation pressure, p_t, static temperature, T, and stagnation temperature, T_t, as shown below:

$$q = \frac{1}{2}\rho V^2, \tag{92}$$

$$\rho = pRT, \tag{93}$$

$$V = M\sqrt{\gamma RT}\,. \tag{94}$$

The static pressure, p, and temperature, T, are determined using the international standard atmosphere model. This model is piecewise continuous, and thus is not included as part of the geometric programming framework and is instead a preprocessing step used to generate the flight conditions at each operating point. The entire mission takes place within the troposphere (under 11,000 meters), however, so a single set of equations can be used. Given the altitude, h, in meters, and the stagnation pressure, p_t, and temperature, T_t, can be determined according to isentropic relations:

$$p = (108.9\ \text{kPa})\left(\frac{(292\ \text{K}) - (0.0065\ \text{K/m})h}{292\ \text{K}}\right)^{-5.256}, \tag{95}$$

$$T = (292\ \text{K}) - (0.0065\ \text{K/m})(h + 610\ \text{m}), \tag{96}$$

$$p_t = p\left(1 + \frac{\gamma - 1}{2}M^2\right)^{\gamma/\gamma - 1}, \tag{97}$$

$$T_t = T\left(1 + \frac{\gamma - 1}{2}M^2\right). \tag{98}$$

For the fixed wing aircraft model, the aircraft flies at constant indicated airspeed, V_{IAS}, and the true airspeed, V_{TAS}, at a given altitude must be calculated for use in the lift, drag, propeller, and engine models. Indicated airspeed can be related to static pressure, p, and dynamic pressure, p_t, of a given flight state and a reference density, ρ_0:

$$V_{\mathrm{IAS}} = \sqrt{\frac{2(p_t - p)}{\rho_0}}, \tag{99}$$

True airspeed can be related to static pressure, p, dynamic pressure, p_t, and temperature T, of a given flight state using isentropic relations:

$$V_{\mathrm{TAS}} = M\sqrt{\gamma RT} \tag{100}$$

$$\frac{p_t}{p} = \left(1 + \frac{\gamma - 1}{2} M^2\right)^{\gamma/(\gamma-1)}, \tag{101}$$

This relation is not GP, so the true airspeed profile is calculated as a preprocessing step to the optimization solution.

2.6.4 Mission Design Variables and Parameters

Tables 2-10 and 2-11 list the symbols and descriptions of the design variables and parameters used in the constraints for the mission models.

Table **2-10**: Mission design variables

	Symbol	Description
Aircraft	R_{climb}	Climb range
	R_{cruise}	Cruise range
	R_{descent}	Descent range
	m_{fuel}	Mission fuel mass (not including reserve)
	m_{res}	Reserve fuel mass
	$\Delta E_{\text{mission}}$	Mission battery energy consumption
	ΔE_{res}	Reserve battery energy consumption
	m_{TO}	Mission takeoff mass
	m_{ZF}	Mission zero-fuel mass
	Δt_{climb}	Climb duration
	m	Instantaneous aircraft mass
	$\dot{m}$	Instantaneous aircraft mass rate of change
	V	Instantaneous aircraft speed
	$\dot{h}$	Instantaneous aircraft climb/descent rate
	$\dot{E}$	Instantaneous aircraft rate of energy usage
	Δm	Sub-segment mass change
	ΔR	Sub-segment distance flown
	Δh	Sub-segment height climbed/descended
	ΔE	Sub-segment energy consumption
Rotorcraft	m_{total}	Total rotorcraft weight at start of segment
	m_{end}	Total rotorcraft weight at end of segment
	m_{ave}	Geometric average rotorcraft weight during segment
	Δm_{fuel}	Rotorcraft mission segment fuel burn
	m_{fuel}	Rotorcraft fuel mass onboard at start of segment
Flight State	q	Dynamic pressure
	V	True airspeed
	ρ	Air density
	T	Static temperature
	T_t	Stagnation temperature
	p	Static pressure
	p_t	Stagnation pressure
	M	Mach number

Table **2-11**: Mission constant parameters

	Symbol	Description	Value
Aircraft	R	Mission range	450 nmi
	m_{pay}	Mission payload mass	7147 lb
	$\Delta t_{\text{climb,max}}$	Maximum time to climb	20 min
	$\Delta t_{\text{reserve}}$	Reserve cruise time	45 min
	$\ell_{\text{TO,max}}$	Maximum takeoff distance	3500 ft
	σ	Air density ratio	1.0
	$C_{L_{\text{TO}}}$	Takeoff lift coefficient	2.7
	Δt_{TO}	Takeoff duration	2 min
	v_{cruise}	Cruise indicated airspeed	237 knots
	h_{cruise}	Cruise altitude	25000 ft
Rotorcraft	m_{pay}	Payload weight	1000 lb
	Δt_{hover1}	Initial hover duration	5 min
	Δt_{cruise}	Cruise duration	60 min
	Δt_{hover2}	Final hover duration	5 min
	h	Rotorcraft altitude	3280 ft

2.7 Optimization Problem Statement

The parallel hybrid electric aircraft and mission model can be expressed as a constrained optimization problem:

minimize	E	
by varying	propulsion system sizing variables,	Table 2-1
	electrical component sizing variables,	Table 2-4
	aircraft sizing variables,	Table 2-7
	mission design variables,	Table 2-10
	propulsion system performance variables,	Table 2-2
	electrical component performance variables,	Table 2-5
	vehicle performance variables,	Table 2-8
subject to	$E \geq m_{\text{batt}}\text{BSE} + m_{\text{fuel}}h_{\text{fuel}}$,	
	propulsion system sizing constraints,	Equations (6), (14), (34), (39)-(41)
	electrical component sizing constraints,	Equations (45), (50), (53), (54)
	vehicle sizing constraints,	Equations (57)-(59) or (63)-(65)
	mission constraints,	Equations (76)-(101)
	propulsion system performance constraints,	Equations (7)-(13), (15)-(35), (37), (38), (42)-(44)
	electrical component performance constraints,	Equations (46)-(49), (51), (52), (55), (56)
	aircraft performance constraints.	Equations (60)-(62), (66)-(75)

(102)

For a given a design mission payload and range, solving (102) will produce the optimal design variable values that minimize the total mission energy, E. The mission consists of 50 segments during climb, 20 segments during cruise, and 5 segments during descent (this discretization was chosen, after a grid convergence study, to achieve error less than 0.1%), the optimization problem contains over 5000 design variables and 9000 constraints. On a single Intel i5 processor core, this optimization problem can be solved in about 20 seconds using GPkit.

In addition to minimizing the total energy for a design mission, the model is also used to evaluate the payload-range capabilities of a design and the energy savings for off-design missions. To do so, the sizing parameters for all of the models are fixed at the value determined by the solution of the design mission, and the performance parameters are left as design variables such that the optimizer finds the optimal performance of the already sized system to minimize the energy consumption. To find the maximum range at a given payload weight, the range is not specified, and the objective function is set to R^{-1} instead of total mission energy, E.

Chapter 3

Fixed Wing Point Design Results and Analysis

In this chapter, we consider the relative performance of conventional and parallel hybrid electric propulsion systems in the context of a canonical regional turboprop aircraft model representative of the de Havilland Canada DHC-8 using the models described in Chapter 2. For design optimizations, parameters listed as design variables (Tables 2-1, 2-2, 2-4, 2-5, 2-7, 2-8, and 2-10) are determined by the optimizer while parameters listed as constants (Tables 2-3, 2-6, 2-9, and 2-11) are held fixed. In Section 3.1, we first consider the performance of a hybrid *retrofit*, comparing the performance of conventional and hybrid propulsion systems powering the same aircraft. In Section 3.2, for a fairer comparison between technologies, we consider the performance of *clean-sheet* designs, optimizing conventional and hybrid propulsion systems *and* aircraft designed for the same mission. In Section 3.3, a summary of the resulting designs is presented, including details of the optimized propulsion system and aircraft sizing and the energy savings provided by hybrid systems. In Section 3.4, we describe the mechanism through which parallel hybrid propulsion enables energy savings by examining the optimal operation of the powertrain throughout the design mission.

3.1 Retrofit Design Comparison

We first consider a so-called *retrofit* design, where the aircraft design is kept constant, and the conventional propulsion system is replaced with a hybrid system. This approach may be representative of early hybrid electric aircraft designs: hybrid-electric propulsion technology may be demonstrated using an existing aircraft [30] or a new hybrid engine option may improve the efficiency of a commercial aircraft at the cost of reduced range [15]. For the baseline conventional (non-electrified) vehicle, we define a design mission with a payload of 85% of the DHC-8 max payload and a range of 900 nautical miles, corresponding to the maximum range of the DHC-8 at that payload. The maximum takeoff weight (MTOW) of the aircraft is provided as a constant parameter in the optimization of both conventional and hybrid designs, and for the latter, the weight of the electrical components effectively reduces the maximum fuel that can be carried and thus the maximum range. We therefore define a design mission with a reduced range of 450 nautical miles to size the hybrid system.

Figure 3-1 shows the so-called *payload-range diagram* for each design and for both state-of-the-art (top figure) and projected (bottom) improvements in electrical components. The vertical axis is the mission payload, and the horizontal axis the mission range. The dashed red and solid blue lines show the maximum payload as a function of range for the conventional and hybrid designs respectively. There are three regimes of the payload-range curve; at low range, the horizontal line represents the maximum structural payload of the aircraft. As range increases, the fuel weight at takeoff increases until the aircraft reaches its maximum takeoff weight. This occurs at the corner of the horizontal

maximum payload line and the first downward sloping line. Along the latter, to further increase the range, the payload must be reduced so that fuel weight can be added at MTOW. The aircraft reaches its maximum fuel capacity at the corner of the two downward sloping lines. To increase the range past this point, payload weight must be reduced.

The color contours show, for the missions both aircraft are capable of, the hybrid energy savings coefficient (ESC), defined as the reduction in total mission energy consumption of the hybrid retrofit aircraft relative to the conventional aircraft:

$$\mathrm{ESC} = \frac{E_{\mathrm{conventional}} - E_{\mathrm{hybrid}}}{E_{\mathrm{conventional}}} \tag{97}$$

At the design point, the hybrid aircraft with state-of-the-art components consumes 7% less energy than the conventional aircraft performing the same mission. The hybrid retrofit aircraft requires 5–12% less total energy depending on the mission; the energy savings increase with decreasing range and decreasing payload, though the energy savings are less sensitive to the latter. The range of the aircraft with no payload, known as the ferry range, is longer for the hybrid aircraft. This is due to the battery energy available in addition to a full fuel tank (the volume of which is assumed unchanged for the retrofit). With advanced electrical components, the trends are similar, but the energy savings benefit is increased to 9–19%.

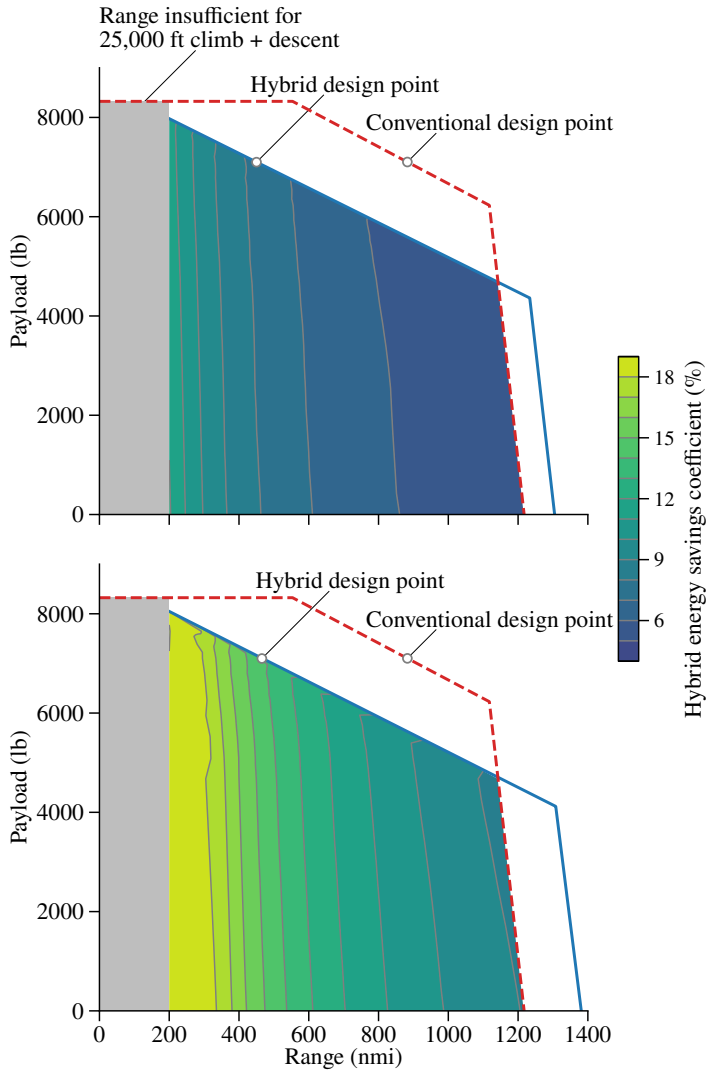

Figure **3-1**: Payload-range capability and hybrid energy savings coefficient for a PHET retrofit compared relative to conventional turboprop baseline with state-of-the-art (top) and advanced (bottom) electrical components

3.2 Clean-Sheet Design Comparison

While the retrofit comparison depicts a possible early implementation of hybrid electric propulsion systems on aircraft, it provides an optimistic view of the energy savings enabled by this technology: a smaller aircraft with a conventional turboprop

propulsion system designed for the reduced range of the retrofit would also be more efficient than the baseline aircraft. A better measure of hybrid propulsion system performance is the hybrid energy savings relative to a vehicle with a conventional propulsion system *designed for the same mission*.

Figure 3-2 shows the same payload-range performance and hybrid energy savings as in Figure 3-1, but for two different aircraft, powered by parallel hybrid electric turboprop (PHET) and conventional turboprop propulsion systems, optimized for the same mission as the hybrid retrofit aircraft just discussed, which we refer to as *clean-sheet* designs. The maximum range for a given payload differs by less than 0.3% between the two designs. The qualitative behavior of the hybrid energy savings is similar to the retrofit case: the hybrid aircraft still is capable of performing missions more efficiently than the conventional aircraft, and mission energy savings increase with decreasing range. The magnitude of the hybrid energy savings, however, is reduced relative to the retrofit comparison: for state-of-the-art electrical components, at the design point, the benefit is less than 1%, and the maximum benefit at short range is roughly 3.5%. At ranges above about 600 nmi, the weight of the hybrid aircraft, which is larger than the conventional design, begins to offset the increase in propulsion system efficiency, and the hybrid aircraft consumes 0.5% more energy than the conventional aircraft at the maximum range of the aircraft. For advanced electrical components, on the other hand, the hybrid system provides energy savings of 8–20%, depending on the mission, with a savings of 14% at the design point.

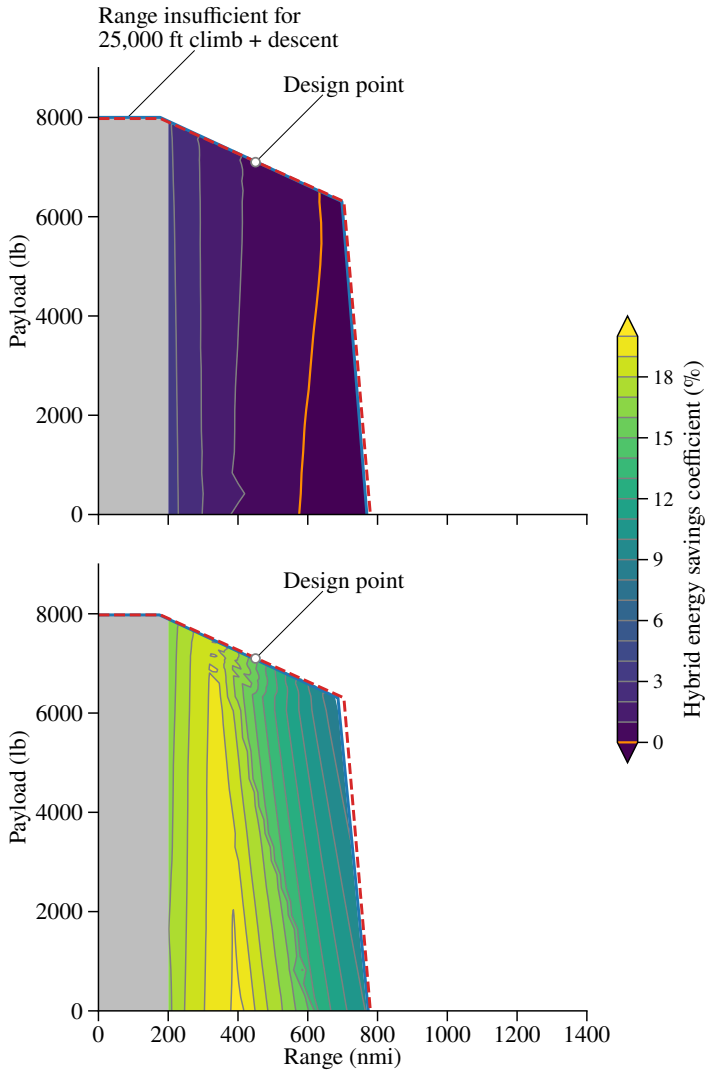

Figure **3-2**: Payload-range capability and hybrid energy savings coefficient for clean-sheet PHET and conventional turboprop designs with state-of-the-art (top) and advanced (bottom) electrical components

3.3 Point Design Summary

Table 3-1 summarizes optimized aircraft and propulsion system weights and mission parameters including fuel burn and electric energy consumption for the hybrid turboprop design mission (450 nautical mile range at 85% maximum DHC-8 payload).

Included in the results are aircraft designed using the projected advanced electrical component technology assumptions in Table 2-1.

Table **3-1**: Summary of fixed-wing aircraft point design results

	Baseline	Hybrid Retrofit		Clean-Sheet Design		
	Conv. Turboprop	State-of-the-art	Advanced	Conv. Turboprop	State-of-the-art Hybrid	Advanced Hybrid
Design range (nmi)	900	450	450	450	450	450
Design payload (lb)	7,147	7,147	7,147	7,147	7,147	7,147
Max takeoff weight (lb)	34,500	34,500	34,500	30,520	33,988	42,172
Empty weight (lb)	22,592	24,460	24,691	20,600	24,091	32,891
Propulsion sys. weight (lb)	1,270	1,436	1,184	1,090	1,411	1,145
Propeller weight (lb)	314	314	314	314	314	314
Gas turbine weight (lb)	693	508	438	486	393	335
Gearbox weight (lb)	263	309	309	290	303	303
Power elec. weight (lb)	-	286	108	-	376	169
Motor weight (lb)	-	19	15	-	25	24
Battery weight (lb)	-	692	1,024	-	653	3,122
Max corr. turb. power (hp)	3,820	3,398	3,157	3,510	3,226	2,655
Max motor power (hp)	-	346	563	-	325	1,081
Cruise turbine efficiency	0.345	0.357	0.353	0.348	0.356	0.349
Mission fuel burn (lb)	**2,175**	**1,976**	**1,759**	**1,925**	**1,882**	**1,390**
Mission total energy consumption (kWh)	**11,803**	**10,899 (-7.7%)**	**10,136 (-14.1%)**	**10,450**	**10,377 (-0.7%)**	**8,994 (-13.9%)**

With state-of-the-art technology, the decrease in gas turbine engine weight does not make up for the added weight of the electric drivetrain, and the total propulsion system weight (which does not include the battery) increases with hybridization. With the projected technology improvements, on the other hand, the improved power density of the electric drivetrain results a net reduction in propulsion system weight for the hybrid retrofit. For the clean-sheet design comparisons, the hybrid electric aircraft are heavier than the conventional aircraft designed for the same mission due to the added weight of the electric drivetrain and battery. For projected improvements in battery specific energy, the weight of the battery *increases* because increasing specific energy and electric drivetrain efficiency allows for more electric energy to be used during the mission.

The retrofit aircraft hybrid energy savings is 7.7% with state-of-the-art technology and 14.1% with advanced technology, relative to the longer-range conventional design.

The clean-sheet design aircraft hybrid energy savings is 0.7% with state-of-the-art technology and 13.9% with advanced technology, relative to the clean-sheet conventional design for the same mission. The baseline conventional aircraft is designed for longer range, and with state-of-the-art technology the retrofit savings are greater than that of the clean-sheet design compared to a conventional aircraft designed for the reduced range. The weight of the clean-sheet design with advanced technology is substantially larger than the other designs because the improved electric component performance enables a greater overall propulsion system efficiency that uses significantly more battery energy; in other words, the introduction of the hybrid propulsion system changes the nature of the system-level design trade between weight and efficiency, and minimizing energy consumption may lead to increased overall weight as electrical component performance improves.

3.4 Mechanisms of Energy Savings

We may gain insight into the mechanism of the energy savings benefit provided by the hybrid systems by examining the optimized operation of the propulsion system throughout the mission for both conventional and hybrid aircraft. Figure 3-3 shows a comparison of the power profiles of both the conventional DHC-8 model and the parallel hybrid retrofit model with state-of-the-art electrical components (the same qualitative behavior is observed for the other designs in Table 3-1).

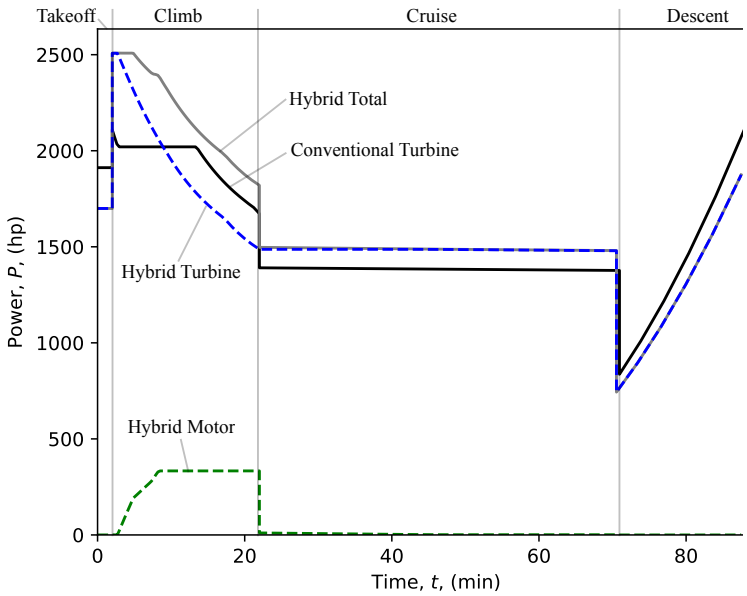

Figure **3-3**: Propulsion system power vs. time; comparison of conventional turbine power to hybrid total, turbine, and motor powers

Throughout climb and cruise, the power of the parallel hybrid electric propulsion system is greater than the power of the conventional turbine due to the larger weight of the hybrid aircraft. At the beginning of climb, the conventional turbine operates at constant power, decreasing near top of climb as the air density decreases, while the hybrid total power requirement decreases steadily throughout climb. The motor is not used at the beginning of climb, and instead ramps up through about the first third of climb until it is operating at its maximum torque for the remainder of climb. In cruise, the powers of both aircraft decrease slightly as the fuel is burned and the aircraft weight decreases. For the hybrid system at the beginning of cruise, a small amount of motor power is used such that the gas turbine operates at constant power throughout cruise despite the decrease in thrust.

The gas generator operates at its maximum efficiency at its maximum corrected power, as described in Section 2.3.2. Any decrease in maximum corrected power improves the efficiency at lower corrected power levels, such as during cruise and descent. Figure 3-4 shows the corrected power of the gas turbine of both propulsion systems and the motor and total shaft power, corrected in the same way, for the hybrid system. Note that the correction factor is not physically relevant to the motor but is applied for consistency.

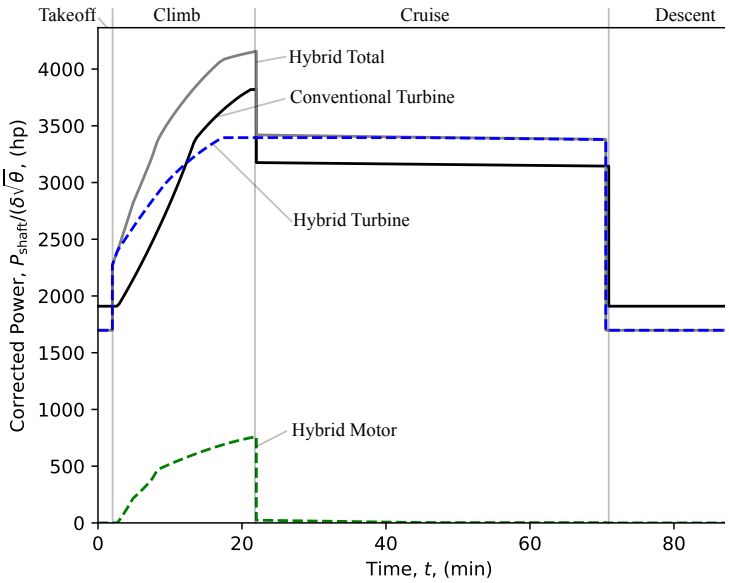

Figure **3-4**: Propulsion system corrected power vs. time; comparison of conventional turbine corrected power to hybrid total, turbine, and motor corrected powers

The motor is used to supplement the gas generator during climb, reducing the gas generator maximum corrected power. During cruise, the hybrid system's gas turbine is operating at its maximum corrected power and thus at higher thermal efficiency, relative to the conventional turboprop. During descent, the gas turbine idle power in the hybrid system is lower than the conventional system because the idle corrected power is allowed

to decrease with the reduction in $P^*_{\max}$, resulting in a fuel burn reduction throughout the descent phase.

The effects of reducing the maximum corrected power on the efficiency throughout the mission can be seen in Figure 3-5.

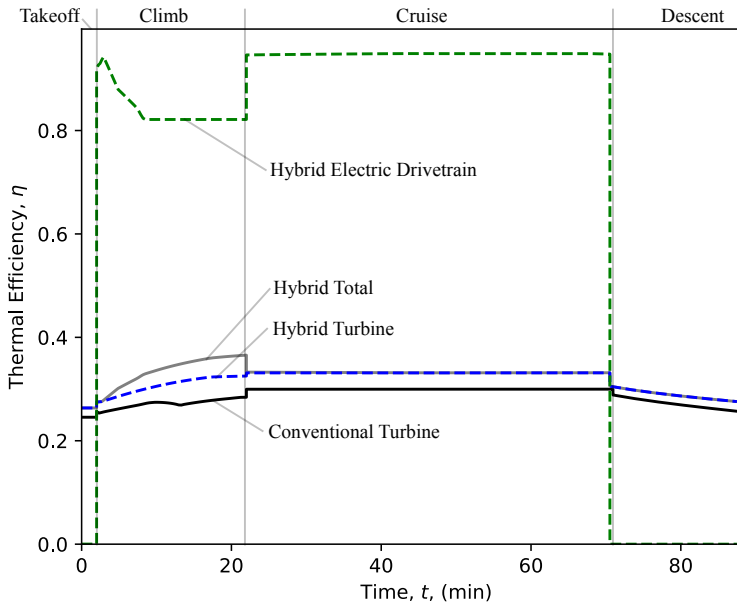

Figure **3-5**: Propulsion system efficiency vs. time; comparison of conventional turbine efficiency to hybrid total, turbine, and electric drivetrain efficiencies

The gas turbine engine in the parallel hybrid electric propulsion system maintains a higher thermal efficiency throughout the entire mission. During climb, some of the required shaft power comes from the motor and the high efficiency of the electric drivetrain further improves the overall efficiency of the propulsion system. The combined effect of changes in drivetrain power and efficiency on propulsion system energy consumption can be seen in Figure 3-6, which shows the rate of fuel and battery energy consumption of both systems.

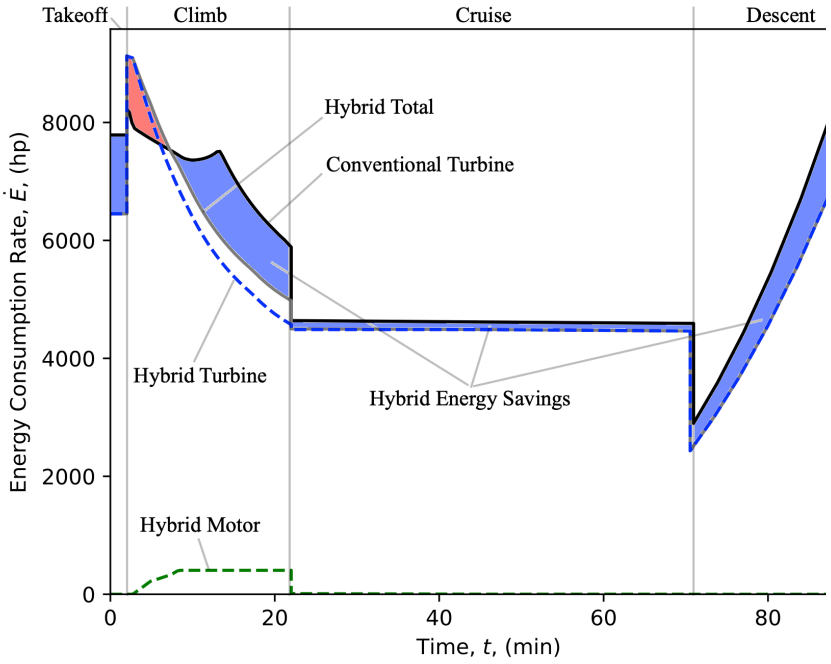

Figure **3-6**: Propulsion system energy consumption rate vs. time; comparison of conventional turbine energy consumption rate to hybrid total, turbine, and motor energy consumption rates

The area under the total power curves represents the total mission energy, and the blue shaded regions between the conventional and hybrid energy consumption curves indicates the total mission energy saved by the latter, while the red shaded region at the beginning of climb indicates a period of increased energy consumption for the hybrid system during this period. During climb, the improvement in efficiency offsets the effect of the increase in total power. During cruise, a small amount of battery energy is used, such that the gas turbine engine operates at constant corrected power as fuel is consumed and thrust decreases, and the thermal efficiency is improved relative to the conventional turboprop. During descent, the fuel burn is reduced due to the reduction in gas turbine engine idle power and improvement in efficiency. In summary, the results show that the

hybrid propulsion system uses battery energy almost entirely during climb but enables energy savings during *all* phases of flight.

Chapter 4

Scaling of Hybrid Energy Savings Benefit

The analysis in Chapter 3 considered five vehicle point designs to quantify a range of hybrid savings and describe the mechanisms of the benefit of the hybrid-electric propulsion architecture. In this chapter, we consider how this benefit *scales* with variations in mission and component technology parameters. Parameter sensitivity analysis indicates that the hybrid-electric vehicle energy consumption is sensitive to design range and battery specific energy, and in Section 4.2, we assess trends in hybrid energy savings with respect to these two parameters. In Section 4.3, we assess the effect of electrical component parameters, representing future advances in battery, power electronics, and machine technology. As shown in Chapter 3, the payload-range energy savings dependence was consistent across technology assumptions, so in this chapter we consider only the performance for the design mission.

4.1 Design Parameter Sensitivities

To better understand how input design parameters affect the solution, we consider the *sensitivities* of the objective function to each parameter. The sensitivity values, listed in Table 4-1 for the clean-sheet hybrid design with assumed state-of-the-art components, are related to the *Lagrange multipliers* of the optimization problem solution, which indicate the local rates of change of the minimized objective with respect to changes in

the design parameters. A positive value indicates an increase in the parameter will result in an increase in the objective function, and a negative value conversely indicates an increase in the parameter will result in a decrease in the objective function. For example, increasing the mission range by 1% would result in an increase to the total energy consumption of about 0.919%. Parameters with large sensitivities can indicate changes in the design or assumptions that can have a large impact on the objective, but this must be weighed against the possible change in the design parameter, which may be limited by design requirements or technological limits.

Table **4-1**: Design parameter sensitivities for clean-sheet hybrid design with assumed state-of-the-art electrical components

	Sensitivity	Value
Range	+0.919	450 nmi
Payload mass	+0.509	7,147 lb
Time to climb	-0.104	20 min
Max turbine inlet temperature	-0.796	1,400 K
Burner pressure ratio	-0.750	0.99
Nozzle pressure ratio	-0.750	0.99
Max compressor pressure ratio	-0.116	15
Max inlet corrected flow	-0.059	0.3625
Max inter-turbine temperature	-0.056	1,058 K
Mass scaling factor	+0.039	19,751 kg/m^3
Battery specific energy	-0.0587	250 Wh/kg
Power electronics specific power	-0.0219	2.2 kW/kg
Battery max discharge rate	-0.0071	10 1/hr
Power electronics efficiency	-0.0051	0.95
Motor internal resistance	-0.0051	50 mΩ
Motor scaling factor	-0.0014	0.33

The results in Table 4-1 show the energy consumption is more sensitive to mission and gas turbine parameters than to the electrical component parameters. This is because the electrical components make up a small fraction of the overall vehicle weight and power: the battery stores just 1.6% of the total mission energy and has a maximum power of 13.7% of the maximum gas turbine power; doubling the battery weight would increase the maximum takeoff weight of the aircraft by less than 2%. The sensitivities,

however, are local, and change with the overall system design; it is therefore instructive to examine the scaling of the hybrid energy savings with improvements in electrical component performance.

4.2 Hybrid Benefit Scaling with Range and BSE

Of the electrical components in the parallel hybrid electric turboprop (PHET) system, the mission energy consumption is most sensitive to the battery specific energy (BSE). BSE is also intrinsically linked to the design range of the vehicle, to which the mission energy is also sensitive: there is a maximum range beyond which, for a given BSE, a turboprop is more energy efficient than a PHET propulsion system. Figure 4-1 shows design mission hybrid energy savings as a function of both range and BSE. At each BSE and range, both a conventional and hybrid aircraft are sized, and the contours show the energy savings coefficient at the design point. Here and in the analyses that follow in this chapter, all other design parameters that are not variables in the figure are held fixed at their baseline state-of-the-art values. As range increases, the effect of the low specific energy of the battery compared to that of jet fuel becomes more significant, compounded by the fact that the fixed weight of the battery must be carried for the entire flight, whereas the fuel weight decreases as it is consumed in the engine. These are the two main factors that cause the energy savings of hybrid aircraft to decrease with increasing range. Increasing BSE, on the other hand, decreases the weight penalty of energy stored in the battery. As a result, improving the specific energy of batteries is seen as an enabling technology for hybrid transport aircraft.

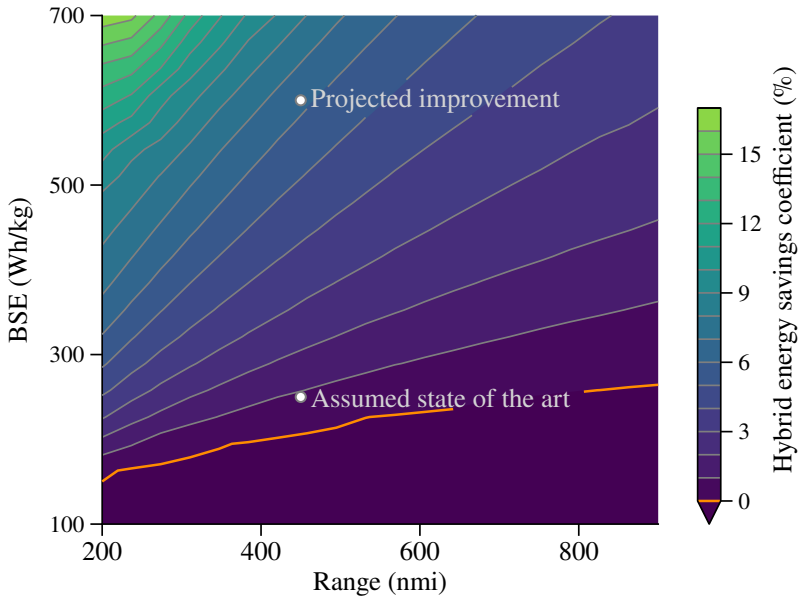

Figure **4-1**: Clean sheet design energy savings vs. battery specific energy and range.

4.3 Hybrid Benefit Scaling with Electrical Component Technology

The main mechanism by which parallel hybrid electric propulsion systems reduce the total mission energy consumption is the reduction in maximum corrected power of the gas turbine engine, resulting in improved efficiency throughout the mission. As electrical component efficiency and specific power increase, the optimal electric drivetrain power increases. Figure 4-2 shows how the percentage of the total propeller shaft power supplied by the motor at top of climb and during cruise vary with battery specific energy with all other electric component parameters held constant at the state-of-the-art values. Using electric power at top of climb is beneficial at a lower battery specific energy for the retrofit aircraft than the clean-sheet design aircraft because the original airframe is oversized for the design mission of the hybrid propulsion system and

thus has unused weight capacity available for the battery. As battery specific energy increases, both aircraft use a small amount of electric power at the start of cruise to further reduce the maximum gas turbine power and increase cruise thermal efficiency. At higher specific energies, it becomes beneficial to use electric power during cruise to take advantage of the high efficiency of the electric drivetrain compared to the gas turbine engine, and the weight penalties of doing so are reduced.

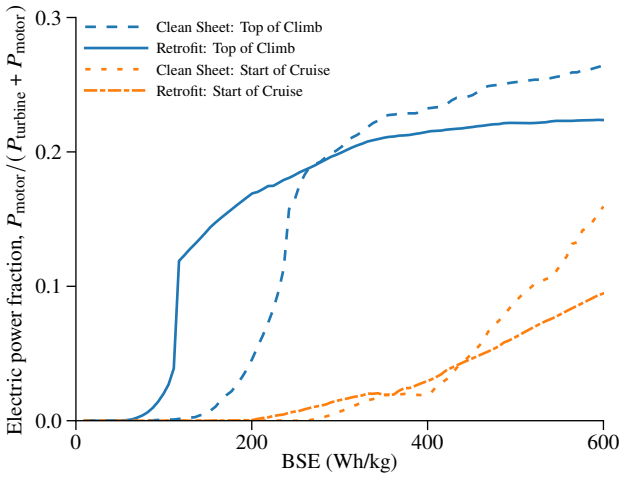

Figure **4-2**: Motor power fraction comparison at top of climb and start of cruise. State-of-the-art batteries enable electrification during climb, while advanced batteries can provide additional power during cruise.

Increasing the specific power of the power electronics and specific torque of the motor provide similar benefits to the system level performance, both leading to an increase of the electric powertrain overall specific power. Figure 4-3 shows the effect of changing the specific power of the power electronics or the specific torque of the motor on the energy savings of a parallel hybrid system over the conventional aircraft. The horizontal axis is the combined specific power of the motor and power electronics, defined as the maximum motor electrical power divided by the sum of their masses. With

state-of-the-art technology assumptions, the power electronics are more than seven times heavier than the motor and only 0.38% of the overall vehicle weight.[2] Increasing the specific torque of the motor therefore provides little weight savings, and mission energy consumption is more sensitive to improvements in the power electronics specific power. The trend in energy savings with combined power density is the same, however, regardless of whether the weight savings come from the motor or the power electronics.

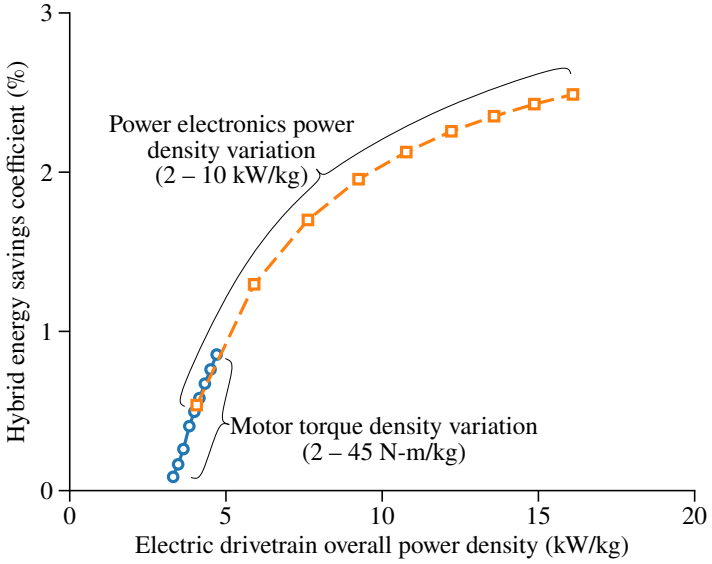

Figure **4-3**: Hybrid energy savings vs. electric drivetrain overall specific power

The motor and power electronics efficiency can also be combined to an overall electric powertrain efficiency representing the losses between the power exiting the battery and the motor shaft power:

[2] The turbine and motor speed are both assumed to be equal to 28,900 RPM, reduced to the propeller shaft speed of 1200 RPM through the gearbox. The high speed of the motor allows it to operate at low torque, improving the specific power of the motor (see Equation (45)).

$$\eta_{\text{elec.drivetrain}} = \eta_{\text{PE}} * \eta_{\text{mot,TOC}} \quad (103)$$

Figure 4-4 shows contours of energy savings as a function of electric powertrain specific power and efficiency. With state-of-the-art technology, the energy consumption of the hybrid aircraft is less sensitive to the powertrain efficiency than to specific power. Because the electric drivetrain contributes a small fraction of the overall propulsive power, reducing losses in the electrical system only slightly improves the system performance. Increasing the specific power of the electric powertrain, on the other hand, allows for system weight reduction, increased electrification, and increased energy savings. Contours levels indicate increasing the electric drivetrain efficiency or specific power results in a lower benefit relative to improvements in battery specific energy seen in Figure 4-3.

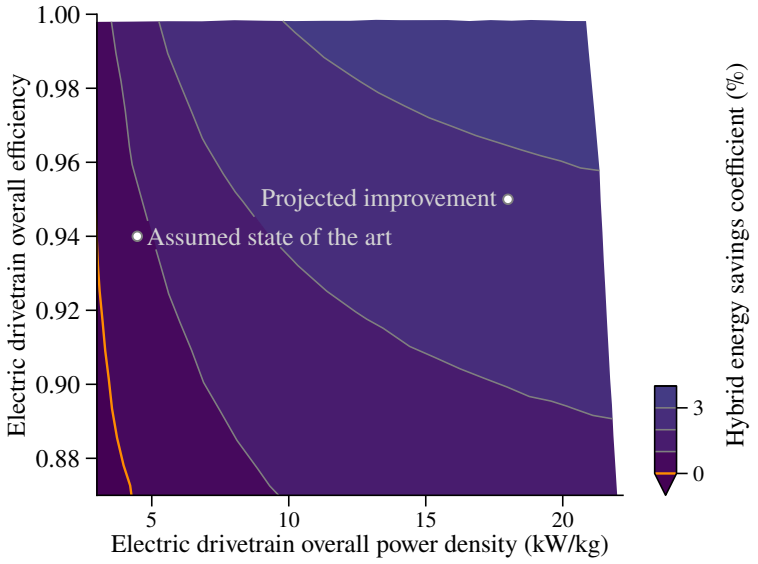

Figure **4-4**: Hybrid energy savings vs. electric drivetrain overall efficiency and specific power.

Figure 4-5 shows energy savings as a function of the battery sizing and performance parameters; the battery specific energy determines the weight of battery energy, while the maximum C-rate determines how efficiently the energy stored in the battery is converted into electrical power. As for the motor and power electronics, the total energy consumption is more sensitive to the battery weight than to its efficiency. Improving battery specific energy enables the greatest improvement in energy savings of the electrical component performance parameters considered. However, batteries require a tradeoff between specific energy and maximum discharge rate; the higher the specific energy of the battery, the lower the maximum discharge rate must be. Although this relationship is not modeled directly here, the trends in Figure 4-5 suggest improvements in BSE are more impactful to hybrid energy savings than changes in maximum C-rate. At maximum C-rates below about 3 hr^{-1}, energy savings are much more sensitive to maximum discharge rate and improvements to battery specific energy only provide minimal energy savings. This is because of the time to climb limit of 20 minutes; if the maximum C-rate is below 3 hr^{-1}, efficiency is effectively limited to 50% at the maximum C-rate, and the battery cannot fully discharge during climb.

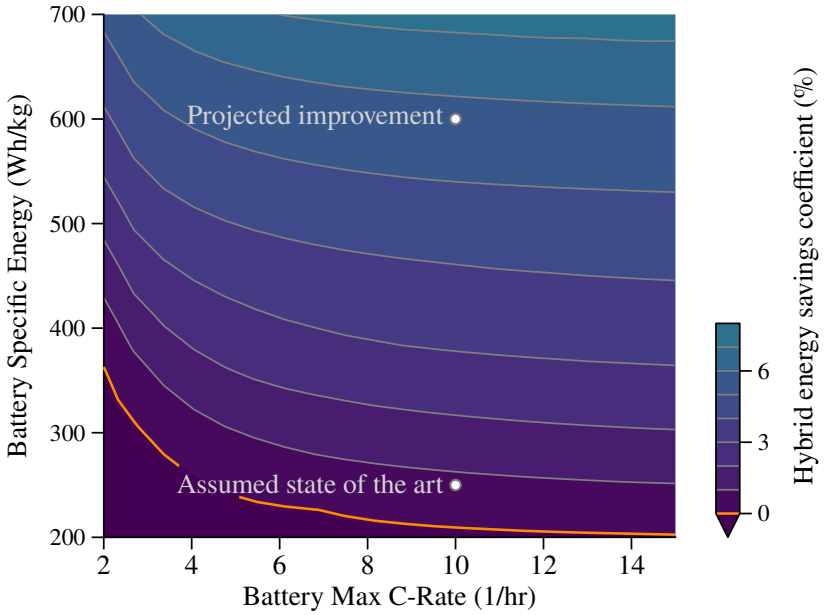

Figure **4-5**: Hybrid energy savings vs. battery specific energy and battery maximum discharge rate.

Chapter 5

Parallel Hybrid Electric Rotorcraft Results and Analysis

In this chapter, we consider the relative performance of conventional and parallel hybrid electric propulsion systems as applied to a notional light aircraft using models described in Chapter 2. For design optimizations, parameters listed as design variables (Tables 2-1, 2-2, 2-4, 2-5, 2-7, 2-8, and 2-10) are determined by the optimizer while parameters listed as constants (Tables 2-3, 2-6, 2-9, and 2-11) are held fixed.

5.1 Point Design Summary

To evaluate the performance benefit of parallel hybrid electric propulsion for rotorcraft, a conventional rotorcraft with a gas turbine engine is compared to the same rotorcraft retrofit with a parallel hybrid propulsion system. Both aircraft perform the same mission: a 5-minute hover, followed by a 60-minute cruise, and another 5-minute hover while carrying a 1000-pound payload. This mission is consistent with operation of rotorcraft for transportation purposes, rather than extended loiter or hover missions that have longer periods of high power requirements. At takeoff, the conventional rotorcraft is less than the maximum takeoff weight, while the hybrid rotorcraft is at its maximum takeoff weight due to the added weight of the electric drivetrain and battery. Table 5-1 summarizes the optimized weights of the rotorcraft and propulsion systems for this

mission, including the conventional design and the hybrid design for state-of-the-art and projected technology assumptions introduced in Table 2-1.

Table **5-1**: Summary of rotorcraft point design results

	Conventional Rotorcraft	State-of-the-art Parallel Hybrid Rotorcraft Retrofit	Advanced Parallel Hybrid Rotorcraft Retrofit
Design range (nmi)	85	85	85
Design payload (lb)	1500	1000	1000
Mission payload (lb)	1000	1000	1000
Max takeoff weight (lb)	5,500	5,500	5,500
Takeoff weight (lb)	4,970	5,500	5,500
Empty weight (lb)	3,583	4,171	4,234
Propulsion sys. weight (lb)	583	743	770
Gas turbine weight (lb)	340	160	101
Gearbox weight (lb)	243	244	244
Power elec. weight (lb)	-	117	147
Motor weight (lb)	-	37	46
Battery weight (lb)	-	427	463
Max corr. turb. power (hp)	1,574	1,250	1004
Max motor power (hp)	-	345	432
Mission fuel burn (lb)	**387**	**329**	**266**
Mission total energy consumption (kWh)	**2,100**	**1,833 (-12.7%)**	**1,569 (-25.3%)**

With both sets of technology of technology assumptions, the propulsion system weight increases relative to the conventional because the added weight of the power electronics and motor are larger than the decrease in the weight of the gas turbine engine. The optimized battery weight is the maximum value, constrained by maximum takeoff weight. Although the battery specific energy, power electronics specific power, and motor mass scaling factor improve with the projected technology assumptions, the weights of these components *increase* due to the increase in the optimized electric drivetrain power and battery energy storage with the change in input technology parameters. Despite the increase in takeoff weight, with state-of-the-art technology assumptions, mission fuel burn is reduced by 15.0% and total mission energy is reduced by 12.7%, relative to the conventional rotorcraft designed for larger payload capabilities.

With projected electrical technology improvements, fuel burn is reduced by 31.3% and total mission energy is reduced by 25.3%, relative to the conventional baseline.

5.2 Mechanisms of Energy Savings

To describe the mechanism of energy savings with the parallel hybrid propulsion system, we first examine the power of the conventional and hybrid rotorcraft systems at different operating points throughout the mission. The gas turbine engine operates at maximum efficiency at its maximum corrected power. Decreasing the maximum power of the engine thus improves the efficiency during lower power phases of flight—in this case, during cruise. Figure 5-1 shows the turbine and motor shaft power of the conventional model and hybrid retrofit model for both state-of-the-art and projected technology assumptions.

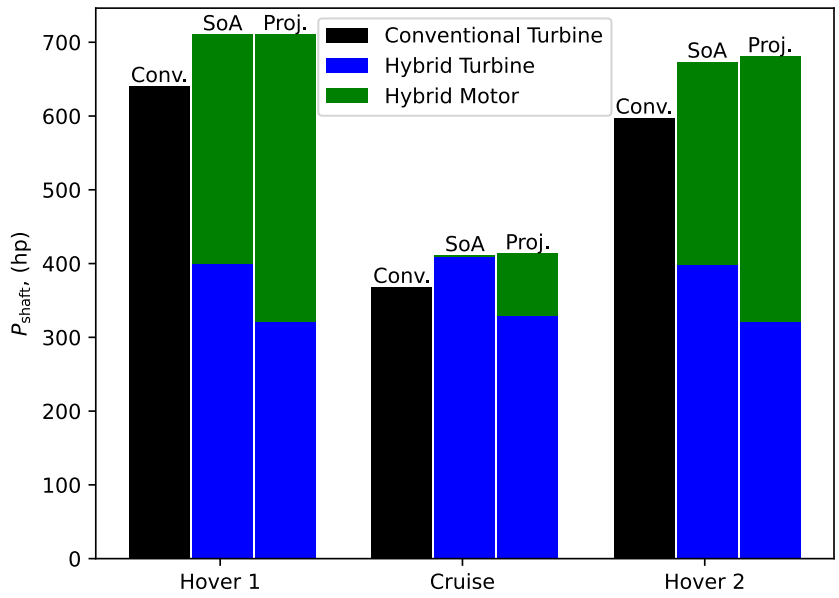

Figure **5-1**: Rotorcraft shaft power for both a conventional gas turbine powered rotorcraft and a parallel hybrid electric rotorcraft with state-of-the-art (middle bar) and projected (right bar) technology assumptions during an initial hover, cruise, and final hover phase.

With-state-of-the-art technology assumptions, the motor provides just under half of the rotor power requirement during the hover segments. The total power during all phases of flight is higher for the hybrid aircraft than for the conventional aircraft because the latter has a lower takeoff weight. By supplementing the gas turbine engine with motor power during hover, the cruise efficiency of the gas turbine engine is improved and the higher efficiency of the motor relative to the gas turbine engine also saves energy during hover, despite higher power requirements. With advanced technology assumptions, electrical power during cruise further reduces the maximum turbine power and improves overall propulsion system efficiency.

The energy usage in each phase of flight is shown in Figure 5-2. The majority of energy is consumed during cruise, which is six times longer than hover, and the majority of energy savings for the hybrid designs occur during cruise. With state-of-the-art technology assumptions, cruise energy savings are mostly a result of the increased gas turbine engine efficiency enabled by cruising at the maximum designed corrected power. With projected technology assumptions, additional cruise energy savings result from the higher efficiency electric drivetrain, which also allows energy savings during hover when the motor supplies about half of the required shaft power.

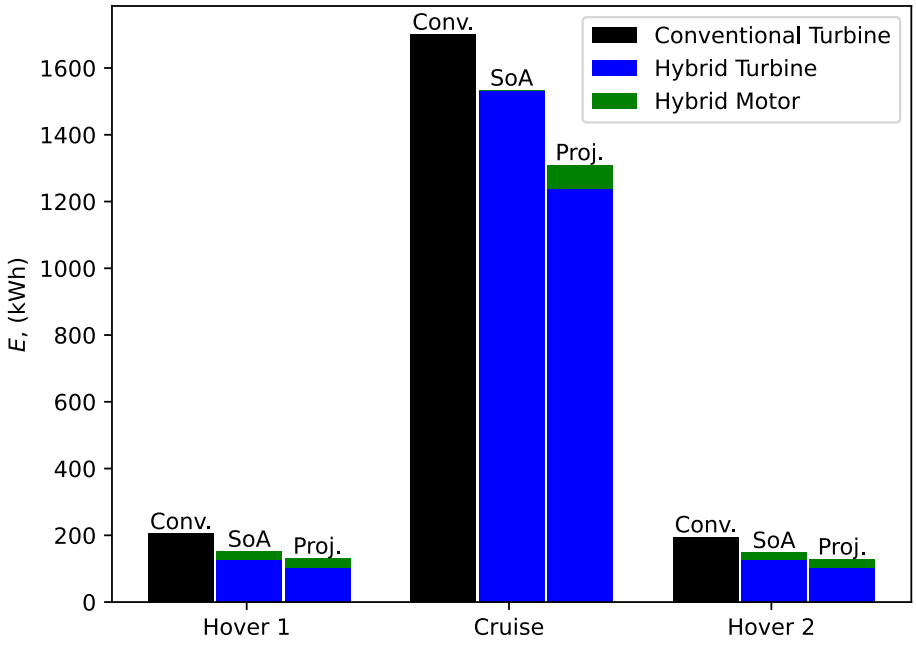

Figure **5-2**: Rotorcraft energy consumption for both a conventional gas turbine powered rotorcraft and a parallel hybrid electric rotorcraft with state-of-the-art (middle bar) and projected (right bar) technology assumptions during an initial hover, cruise, and final hover phase.

Reductions in maximum gas turbine engine power are possible with a small amount of electrical energy storage used during short-duration hover, which enables energy savings. For missions where hover is a larger fraction of the mission duration, the optimized weight of the battery would increase for a given motor power requirement and limit the reduction in the maximum corrected power of the engine and thus the energy savings. Parallel hybrid electric propulsion may be beneficial for rotorcraft and aircraft designed for very short periods of high power requirements followed by lower power long duration cruise phases than for those designed for extended hover or loiter phases.

5.3 Sensitivity of Energy Consumption

To better understand how the constant parameters affect the solution, we examine the sensitivities of the objective function to various parameters in Table 5-2.

Table **5-2**: Design parameter sensitivities for hybrid rotorcraft design with assumed state-of-the-art electrical components

	Sensitivity	Value
Cruise duration	+0.89	60 min
Hover duration	+0.27	10 min
Payload mass	+0.11	1,000 lb
Burner pressure ratio	-1.4	0.99
Nozzle pressure ratio	-1.4	0.99
Max compressor pressure ratio	-0.76	3.5
Max turbine inlet temperature	-0.41	1,400 K
Max inter-turbine temperature	-0.41	1,058 K
Max inlet corrected flow	-0.0086	0.3625
Mass scaling factor	+0.047	8,000 kg/m^3
Battery specific energy	-0.13	250 Wh/kg
Power electronics specific power	-0.076	2.2 kW/kg
Battery max discharge rate	-0.026	10 1/hr
Power electronics efficiency	-0.012	0.95
Motor internal resistance	+0.010	50 mΩ
Motor scaling factor	-0.0024	0.33

Similar to fixed-wing aircraft, the state-of-the-art hybrid design is sensitive to the mission duration, which is effectively the mission range as the cruise speed is constant. The majority of the total mission energy comes from the gas turbine engine, and thus the total energy is more sensitive to turbine parameters than electric drivetrain parameters. Of the electrical parameters, the total mission energy is again most sensitive to the battery specific energy followed by the power electronics specific power. This indicates that the weight of the battery and electric drivetrain is the most important technology parameter for achieving energy savings. Overall, the sensitivities are similar for rotorcraft and fixed-wing aircraft, and the energy consumption is more sensitive to electrical technology parameters due to the increased power fraction of the electric drivetrain.

Chapter 6

Conclusion

6.1 Summary

As commercial aviation associated carbon emissions grow, electrified aircraft propulsion has been proposed as a way to improve efficiency and reduce environmental impact of aircraft. A hybrid electric transport aircraft design optimization model has been developed and applied to parallel hybrid electric aircraft propulsion system design space exploration. The model was used to better understand the mechanisms of energy consumption reduction with parallel hybrid electric propulsion. Energy savings were quantified for two comparison cases: a conventional regional transport turboprop aircraft retrofit with a parallel hybrid electric propulsion system for a reduced range mission, and two aircraft, one with a conventional gas turbine engine and one with a parallel hybrid propulsion system, each designed for the same mission. The model was also used to assess the local sensitivity of the mission energy consumption to mission and technology parameters; trade studies were performed to better understand how changes and improvements in the most sensitive parameters affect the energy savings potential of parallel hybrid electric propulsion systems. The energy savings potential of parallel hybrid electric propulsion was also evaluated for light rotorcraft.

6.2 Conclusions

1. For a regional turboprop retrofit with a parallel hybrid electric propulsion system with state-of-the-art electrical component performance, the hybrid system yields energy savings of 7.7%. When designing new regional transport aircraft to support hybrid propulsion systems, this benefit is reduced to 0.7% relative to a conventional turboprop designed for the same mission.
2. Improvements in electrical component efficiency and specific power or energy can increase the benefit up to 14% for the projected improvements considered in this study.
3. Energy savings are enabled by reducing the peak power requirements for the gas turbine engine by supplementing it with motor shaft power during climb. This improves the thermal efficiency and total energy consumption of the engine *throughout the entire mission*. During climb, the efficient electric drivetrain saves energy over a gas turbine engine. During cruise, the improvement in gas turbine efficiency allows energy savings despite increased aircraft weight. During descent, decreased engine idle fuel burn allows further energy savings.
4. Parallel hybrid electric propulsion systems are capable of saving more energy the shorter the design mission range is, making it a potential solution for regional turboprops and smaller classes of aircraft. The results suggest parallel hybrid electric propulsion may not be beneficial for longer-range aircraft such as the single-aisle and twin-aisle turbofans that represent the majority of commercial aviation today.

5. For light rotorcraft with short duration periods of high thrust, parallel hybrid electric propulsion yields energy savings of 12.7% with state-of-the-art technology and up to 25.3% with projected technology improvements.
6. Similar to fixed-wing aircraft, energy savings for hybrid rotorcraft are enabled by using the electric drivetrain to reduce the peak power requirement of the gas turbine engine, and energy is saved *throughout the entire mission*. During hover, the efficiency electric drivetrain saves energy over a gas turbine engine. During cruise, the improvement in gas turbine efficiency enabled by reducing its peak corrected power allows energy savings despite increased rotorcraft weight. The difference between peak and cruise power is larger for rotorcraft than fixed-wing aircraft, enabling greater energy savings potential for rotorcraft. Parallel hybrid electric propulsion is more beneficial for rotorcraft designed for shorter-duration hover missions because a lighter battery can be used to enable the same cruise efficiency improvement.
7. Improving electrical component efficiencies with new technologies improves the potential energy savings capability of hybrid systems, but the key enabler is reducing the weight of the battery and electric powertrain through improvements to battery specific energy and power electronics and motor specific power.

6.3 Future Work

6.3.1 Component Modeling

The models developed for this study use simplified component models to enable vehicle and propulsion system conceptual design space exploration, scaling studies, and off-design performance analysis. This approach provides a clear identification of enabling technologies to improve the performance of hybrid propulsion systems and for furthering modeling capabilities to better understand their optimal operation and potential benefits. The results showed off-design gas turbine engine performance is central to the energy savings provided by hybrid propulsion systems, and implementing a higher-fidelity gas turbine engine and electrical component performance models, beyond the capability of the present optimization framework, are recommended for more detailed assessment of the benefits for specific vehicle concepts.

6.3.2 Thermal Management

The current model does not describe propulsion system thermal management, but we may comment briefly on the implications of the results in this area. Unlike gas turbine engines, where waste heat is rejected as hot exhaust gas, separate cooling systems will be needed to remove heat generated in the electrical components. The optimized power profile, however, exhibits features that may reduce the size and loss associated with a thermal management system, namely, the electrical components account for about 20% overall propulsion system power, and it is used for a short duration during the later stages

of climb. The hybrid rotorcraft design with state-of-the-art technology operates similarly, with relatively low electrical energy consumption. In the current context, we expect its impact on the optimized power profile and resulting hybrid energy savings to be small, but the details of the thermal management strategy for such systems is an important area for future research.

6.3.3 Hybrid Rotorcraft Propulsion

The results indicate that parallel hybrid electric propulsion may provide significant energy savings for rotorcraft. To better characterize the magnitude and mechanisms of potential energy savings, higher fidelity rotor performance models could be used, allowing cruise speed and altitude to be included as optimization design variables rather than constants. Additionally, rotorcraft are utilized for their ability to perform a variety of missions, such as transport of cargo or passengers, search-and-rescue, and disaster response. Improved mission modeling, such as the discretized model used for fixed-wing aircraft modeling that accounts for climb, descent, and acceleration of the vehicle, could help to better understand how the design of the parallel hybrid propulsion system changes under varied mission requirements. Full or partial power out failures are also an important design consideration, and the potential benefits or drawbacks of parallel hybrid propulsion could be studied in the future.

Similar to the synergy between electrified aircraft concepts and propulsion-airframe integration in fixed-wing aircraft, electrified propulsion systems may synergize well with a multitude of rotorcraft and propulsion system architecture variations. Having

electrical power onboard may allow replacement of the long driveshaft through the tail with lighter cabling and an electric motor to power an antitorque tail rotor or pusher propeller. Suitability of parallel hybrid propulsion systems for missions with high-power conditions during takeoff and hover and long low-power cruise phases lends itself to use on tilt-rotor designs with improved cruise performance. Other electrified propulsion systems such as series hybrid and turboelectric may be beneficial for certain architectures of rotorcraft. Overall, investigating combinations of rotorcraft and propulsion system architectures may reveal other niches where electrified propulsion is even more beneficial.

Once potentially beneficial architectures are identified by conceptual design exploration, propulsion systems can be modeled physically using motors, generators, and programmable loads. As the time-scale of the transient behavior of motors tends to be shorter than gas turbines, motors can be controlled to simulate the behavior of the gas turbine engine in a hybrid system. This physical modeling could provide a better understanding of the dynamics of electrified propulsion systems.

References

[1] E. Terrenoire, D. A. Hauglustaine, T. Gasser, and O. Penanhoat, "The contribution of carbon dioxide emissions from the aviation sector to future climate change," *Environmental Research Letters*, Vol. 14, No. 8, Jul. 2019.

[2] National Academies of Science, Engineering, and Medicine, *Commercial Aircraft Propulsion and Energy Systems Research: Reducing Global Carbon Emissions*, Washington: National Academies Press, 2016.

[3] V. Viswanathan, A. H. Epstein, Y.M. Chiang, E. Takeuchi, M. Bradley, J. Langford, and M. Winter, "The challenges and opportunities of battery-powered flight," Nature, Vol. 607, No. 7894, pp. 519–525, Jan, 2022.

[4] A. H. Epstein and S. M. O'Flarity, "Considerations for Reducing Aviation's CO2 with Aircraft Electric Propulsion," *Journal of Propulsion and Power*, Vol. 35, No. 3, pp. 572–582, May, 2019.

[5] D. K. Hall, E. M. Greitzer, A. P. Dowdle, J. J. Gonzalez, W. W. Hoburg, J. H. Lang, J. S. Sabnis, Z. S. Spakovszky, B. Yutko, C. Courtin, W. Thalheimer, L. Trollinger, J. Tylko, N. Varney, A. Uranga, S. Byahut, and M. Kruger, "Feasibility of Electrified Propulsion for Ultra-Efficient Commercial Aircraft, Final Report," NASA/CR–2019-220382, Dec. 2019.

[6] J. S. Langford and D. K. Hall, "Electrified Aircraft Propulsion," *The Bridge*, Vol. 50, No. 2, pp. 21–27, Jun. 2020.

[7] Fuel Cells and Hydrogen 2 Joint Undertaking, "Hydrogen-powered aviation: a fact-based study of hydrogen technology, economics, and climate impact by 2050," Publications Office of the European Union, Jul. 2020.

[8] R. de Vries, M. Hoogreef, and R. Vos, "Aero-Propulsive Efficiency Requirements for Turboelectric Transport Aircraft," AIAA SciTech Forum, AIAA Paper No. 2020-0502, Jan. 2020.

[9] M. Kruger, S. Byahut, A. Uranga, A. Dowdle, J. Gonzalez, and D.K.Hall, "Electrified Aircraft Trade-Space Exploration," AIAA AVIATION Forum, AIAA Paper No. 2018-4227, Jun. 2018.

[10] D. L. Simon, J. W. Connolly, and D. E. Cully, "Control Technology Needs for Electrified Aircraft Propulsion Systems," *Journal of Engineering for Gas Turbines and Power*, Vol. 142, No. 1, Jan. 2020.

[11] H. Richter, J. W. Connolly, and D. L. Simon, "Optimal Control and Energy Management for Hybrid Gas-Electric Propulsion," *Journal of Engineering for Gas Turbines and Power*, Vol. 142, No. 9, Sep. 2020.

[12] D. F. Finger, C. Braun, and C. Bil, "Comparative Assessment of Parallel-Hybrid-Electric Propulsion Systems for Four Different Aircraft," *Journal of Aircraft*, Vol. 57, No. 5, pp. 843–853, Sep. 2020.

[13] M. K. Bradley and C. K. Droney, "Subsonic Ultra Green Aircraft Research: Phase I Final Report," NASA/CR–2011-216847, Apr. 2011.

[14] M. K. Bradley and C. K. Droney, "Subsonic Ultra Green Aircraft Research: Phase II – Volume II – Hybrid Electric Design Exploration," NASA/CR–2015-218704/Volume II, Apr. 2015.

[15] C. Lents and L. Hardin, “Fuel Burn and Energy Consumption Reductions of a Single-Aisle Class Parallel Hybrid Propulsion System,” AIAA Propulsion and Energy Forum, AIAA Paper No. 2019-4396, Aug. 2019.

[16] T. Spierling and C. Lents, “Parallel Hybrid Propulsion System for a Regional Turboprop: Conceptual Design and Benefits Analysis,” AIAA Propulsion and Energy Forum, AIAA Paper No. 2019-4466, Aug. 2019.

[17] R. A. Danis, M. W. Green, J. L. Freeman, and D. W. Hall, “Examining the Conceptual Design Process for Future Hybrid-Electric Rotorcraft,” NASA/CR–2018–219897, May 2018.

[18] C. A. Saias, I. Goulos, I. Roumeliotis, V. Pachidis, and M Bacic, “Preliminary Design of Hybrid-Electric Propulsion Systems for Emerging Urban Air Mobility Rotorcraft Architectures,” *Journal of Engineering for Gas Turbines and Power*, Vol. 143, No. 11, Nov. 2021.

[19] P. G. Kirschen, M. A. York, B. Ozturk, and W. W. Hoburg, “Application of Signomial Programming to Aircraft Design,” *Journal of Aircraft*, Vol. 55, No. 3, pp. 965–987, May 2018.¨

[20] M. A. York, B. Ozturk, E. Burnell, and W. W. Hoburg, “Efficient Aircraft Multidisciplinary Design Optimization and Sensitivity Analysis via Signomial Programming,” *AIAA Journal*, Vol. 56, No. 11, pp. 4546, Nov. 2018.

[21] M. J. Burton, M. Drela, C. Courtin, D. Colas, V. S. Suryakumar, and N. H. Roberts, “Solar Aircraft Design Trade Studies Using Geometric Programming,” AIAA AVIATION Forum, AIAA Paper No. 2018-3740, Jun. 2018.

[22] C. Courtin, M. Burton, P. Butler, A. Yu, P. Vascik, and J. Hansman, "Feasibility Study of Short Takeoff and Landing Urban Air Mobility Vehicles using Geometric Programming," AIAA AVIATION FORUM, AIAA Paper No. 2018-4151, Jun. 2018.

[23] A.P. Dowdle, D.K. Hall, and J.H. Lang, "Electric Propulsion Architecture Assessment via Signomial Programming," AIAA/IEEE Electric Aircraft Technologies Symposium, AIAA Paper No. 2018-5026, Jul. 2018.

[24] W. Hoburg and P. Abbeel, "Geometric Programming for Aircraft Design Optimization," *AIAA Journal*, Vol. 52, No. 11, pp. 2414–2426, Nov. 2014.

[25] E. Burnell, N. B. Damen, and W. Hoburg, "GPkit: A Human-Centered Approach to Convex Optimization in Engineering Design," in Proceedings of the 2020 CHI Conference on Human Factors in Computing Systems, 2020.

[26] W. Johnson, "NDARC - NASA Design and Analysis of Rotorcraft," NASA/TP–2015–218751, Apr. 2015.

[27] M. Duffy, A. Sevier, R. Hupp, E. Perdomo, and S. Wakayama, "Propulsion Scaling Methods in the Era of Electric Flight," AIAA Paper No. 2018-4978, Jul. 2018.

[28] D.P. Raymer, *Aircraft Design: A Conceptual Approach*, Fifth Edition, Reston, Virginia: American Institute of Aeronautics and Astronautics, 2012.

[29] W. Johnson, *Helicopter Theory*, Dover Publications, 1994.

[30] R. Salter, J. Falcone, and J. Bonet, "Parallel Hybrid Electric Propulsion Demonstrator Concept," AIAA SciTech Forum, AIAA Paper No. 20121-0260, Jan. 2021.